Biochemical characterization of the mouse ABCF3 protein, a partner of the flavivirus-resistance protein OAS1B

Received for publication, March 15, 2019, and in revised form, August 12, 2019 Published, Papers in Press, August 14, 2019, DOI 10.1074/jbc.RA119.008477

Elizabeth Peterson, Emma Shippee, Margo A. Brinton, and Parjit Kaur[1]

From the Department of Biology, Georgia State University, Atlanta, Georgia 30303

Edited by Charles E. Samuel

Mammalian ATP-binding cassette (ABC) subfamily F member 3 (ABCF3) is a class 2 ABC protein that has previously been identified as a partner of the mouse flavivirus resistance protein 2′,5′-oligoadenylate synthetase 1B (OAS1B). The functions and natural substrates of ABCF3 are not known. In this study, analysis of purified ABCF3 showed that it is an active ATPase, and binding analyses with a fluorescent ATP analog suggested unequal contributions by the two nucleotide-binding domains. We further showed that ABCF3 activity is increased by lipids, including sphingosine, sphingomyelin, platelet-activating factor, and lysophosphatidylcholine. However, cholesterol inhibited ABCF3 activity, whereas alkyl ether lipids either inhibited or resulted in a biphasic response, suggesting small changes in lipid structure differentially affect ABCF3 activity. Point mutations in the two nucleotide-binding domains of ABCF3 affected sphingosine-stimulated ATPase activity differently, further supporting different roles for the two catalytic pockets. We propose a model in which pocket 1 is the site of basal catalysis, whereas pocket 2 engages in ligand-stimulated ATP hydrolysis. Co-localization of the ABCF3–OAS1B complex to the virus-remodeled endoplasmic reticulum membrane has been shown before. We also noted that co-expression of ABCF3 and OAS1B in bacteria alleviated growth inhibition caused by expression of OAS1B alone, and ABCF3 significantly enhanced OAS1B levels, indirectly showing interaction between these two proteins in bacterial cells. As viral RNA synthesis requires large amounts of ATP, we conclude that lipid-stimulated ATP hydrolysis may contribute to the reduction in viral RNA production characteristic of the flavivirus resistance phenotype.

Members of the genus *Flavivirus* in the family Flaviviridae include human pathogens, such as West Nile virus (WNV),[2] Japanese encephalitis virus, tick-borne encephalitis virus, yellow fever virus, dengue virus, and Zika virus. Phenotypic evidence of genetically controlled host resistance to particular virus pathogens has previously been obtained, but few of the genes involved have been identified and characterized (1). Flavivirus resistance and susceptibility in mice are controlled by the alleles of the *Flv* locus, which encode the 2′–5′-oligoadenylate synthetase (OAS) 1B protein. Flavivirus-resistant mice express a full-length OAS1B protein, while susceptible mice produce a truncated protein (OAS1B-tr) due to the presence of a premature stop codon (2, 3). *oas1* genes are components of the cellular innate immune response that when activated by viral dsRNA synthesize short 2′–5′-linked oligoadenylates (2–5A). These bind to cytoplasmic RNase L causing it to dimerize and cleave single-stranded cell and viral RNAs (4). Eight orthologs of the *oas1* gene (*oas1a–h*) have been identified in mice (5, 6). The proteins produced by only two of the murine *oas1* genes (OAS1A and OAS1G) are active synthetases. OAS1B is an inactive synthetase that cannot produce 2–5A (7, 8).

The OAS1B protein localizes to the endoplasmic reticulum (ER) through a C-terminal transmembrane domain consisting of 23 amino acid residues (9). OAS1B-tr, the truncated version of OAS1B, lacks this C-terminal transmembrane domain and is therefore unable to anchor to the ER. Flavivirus RNA replication occurs within invaginations in the ER membrane (10). Although flaviviruses can attach and enter resistant and susceptible mouse cells with similar efficiency, resistant cells produce reduced levels of intracellular flavivirus RNA as well as lower virus yields (9). A yeast two-hybrid screen of a mouse brain library identified two binding partners for OAS1B: ABCF3, which belongs to class 2 of the ATP-binding cassette (ABC) superfamily of proteins; and ORP1L, a protein involved in sterol binding and regulation of late endosome motility as well as protein and lipid transport (9, 11). Interaction between OAS1B and ABCF3 was further demonstrated by co-immunoprecipitation in mammalian lysates and co-localization in baby hamster kidney cells by fluorescence microscopy (9). Knockdown of ABCF3 protein levels increased WNV yields but not those of two nonflaviviruses, vesicular stomatitis virus and Sindbis virus, supporting a specific role for ABCF3 in OAS1B-mediated flavivirus resistance (9). Moreover, the flavivirus-specific effect of knockdown of ABCF3 was only seen in resistant mouse embryo fibroblasts (MEFs) that naturally express the full-

This work was supported by USPHS National Institutes of Health Grant 5R01AI045135-12 from NIAID (to M. A. B. and P. K.) and by a graduate fellowship from Georgia State University (to E. P.). The authors declare that they have no conflicts of interest with the contents of this article. The content is solely the responsibility of the authors and does not necessarily represent the official views of the National Institutes of Health.

This article contains Figs. S1–S4.

[1] To whom correspondence should be addressed. Tel.: 404-413-5405; E-mail: pkaur@gsu.edu.

[2] The abbreviations used are: WNV, West Nile virus; ER, endoplasmic reticulum; ABC, ATP-binding cassette superfamily; NBD, nucleotide-binding domain; TMD, transmembrane domain; PAF, platelet-activating factor; LPC, lysophosphatidylcholine; LPI, lysophosphatidylinositol; TNP-ATP, 2′(3′)-*O*-(2,4,6-trinitrophenyl)adenosine 5′-triphosphate; NATA, *N*-acetyl-L-tryptophanamide; Ni-NTA, nickel-nitrilotriacetic acid; PE, phosphatidylethanolamine; MEF, mouse embryo fibroblast; OAS1B-tr, OAS1B-truncated; 2–5A, 2′–5′-linked oligoadenylate; P, pocket; IPTG, isopropyl 1-thio-β-D-galactopyranoside; IB, inclusion body.

length OAS1B protein and not in susceptible MEFs expressing the truncated OAS1B-tr (9).

Most ABC proteins contain two nucleotide-binding domains (NBDs) and two transmembrane domains (TMDs) that are present either in the same polypeptide or on separate subunits. The NBDs contain several conserved motifs, including Walker A, Walker B, ABC Signature, Q-loop, and Switch motifs, and the TMDs have limited sequence conservation (12). The Walker A motif of ABC proteins plays a critical role in ATP binding, and Walker B is involved in hydrolysis (12). Analyses of the crystal structures of ABC proteins suggest that their ATP-binding pockets are located at the interface formed by the Walker A motif of one NBD juxtaposed against the signature motif of the other NBD in a head–to–tail configuration (12, 13). ABC proteins are normally involved in the cellular transport of a diverse range of substrates in both prokaryotes and eukaryotes, and this process is coupled to the energy of ATP hydrolysis (14, 15). Members of the ABC superfamily are divided into three classes (14, 15). Although the function, mechanism, and structure of class 1 and class 3 proteins have been elucidated in detail (14, 15), little is known about class 2 proteins and their physiological roles. Class 2 proteins are distinct in that they lack the TMD domains but contain two tandemly-linked NBD domains, which also likely participate in a head–to–tail configuration resulting in two ATP-binding pockets (13). Because of the lack of a transmembrane domain, the primary cellular role of most class 2 proteins is believed to be regulatory in nature (15). It has been postulated that some class 2 proteins may complex with other cellular membrane proteins to enable them to transport ligands. The bacterial Mel protein that interacts with the proton-motive force– driven transmembrane pump protein MefE to form a complex involved in the transport of erythromycin is the single example of such a complex available to date (16, 17).

The ABC proteins have also been assigned to eight subfamilies, A–H. Subfamilies E and F, which do not contain TMDs, belong to ABC class 2 (15). Subgroup F includes mammalian F1, F2, and F3; yeast GCN20 and EF3; and bacterial EttA, Vga(A), and Uup proteins. Some bacterial ABCF proteins, such as Vga(A), confer antibiotic resistance by drug displacement at the peptidyl transferase center of the ribosome (18–22). EttA, which functions as a translation factor and regulates progression of the 70S initiation complexes into the elongation cycle, also associates with the ribosome (23, 24). Association with the ribosome was also reported for other ABCF proteins, including mammalian ABCF1 (ABC50) and yeast EF3, ARB1 (ABCF2), and GCN20 (ABCF3) proteins, which regulate protein translation either at the level of initiation or elongation (25–33). Additional reports suggesting that the eukaryotic F1, F2, and F3 proteins can impact diverse cellular activities, including innate immunity against retroviruses (34), promotion of phagocytosis (35), anti-apoptotic effect (36), and co-localization with a tumor-inducing protein (37) are also available; however, there is no firm consensus about their cellular functions, and none have been characterized biochemically. However, data from limited biochemical analyses of the bacterial ABCF proteins Vga(A), Uup, and EttA are available. All three of these bacterial ABCF proteins have ATPase activity, which was shown to be essential for their function in the cell (23, 38, 39). The ATPase activity of Vga(A) was found to be inhibited by the antibiotic pristinamycin IIA (38), suggesting direct binding of Vga(A) with its ligand, although there is no known partner protein with a TMD. By contrast, ABC proteins belonging to class 1 and 3 normally bind their ligands only when in complex with their cognate TMD partner proteins (14). Finally, the bacterial ABCF proteins also have about an 80-amino acid long inter-ABC domain linker, which contains conserved sequences and is rich in positively-charged residues (40). In the case of Vga(A) and EttA, the linker region was shown, by mutagenesis and deletion analysis, to be critical for their association with the ribosome and for their function (20, 21, 23). Interestingly, association of the EttA linker with the ribosome was found to be sensitive to the ATP/ADP ratio, leading to the proposal that this protein plays a role in regulation of protein chain elongation in energy-starved cells (23).

To gain an understanding of mammalian ABCF3 protein functions that may play a role in the OAS1B-mediated flavivirus-resistance mechanism, the ATP-binding and ATPase activities of mouse ABCF3 were characterized, potential ligands of ABCF3 were identified, and the ability of ABCF3 to interact with OAS1B in bacterial cells was analyzed. We showed that purified ABCF3 protein is an active ATPase with both NBDs contributing to the catalytic activity. TNP-ATP binding studies showed that the two NBDs of ABCF3 are asymmetric with NBD2 playing a more important role in nucleotide binding. The substrates of the ABCF3 protein are currently not known. However, many ABC family proteins are known to transport lipids and amphiphilic drugs, and their ATPase activities have been shown to be stimulated or inhibited by these substrates (41–49). Moreover, flavivirus infections modulate host cell lipid metabolism (50) and result in changes in the levels of fatty acids, phospholipids, sphingolipids, and cholesterol in cell membranes (51–53), including in the ER, which is the site of OAS1B/ABCF3 localization and a major site for lipid biosynthesis (9, 54). Therefore, in this study we tested the effect of multiple lipids and amphiphilic drugs on ABCF3 activity. Interestingly, the ATPase activity of ABCF3 was found to be modulated by several of the tested lipids, but not by amphiphilic drugs. The basal and lipid-stimulated ATPase activity data obtained with ABCF3 mutated in NBD1 and NBD2 suggested that the two ATP-binding pockets may play different roles in ATP hydrolysis. Co-expression of *abcf3* and *oas1b* in bacteria resulted in alleviation of growth inhibition caused by *oas1b* expression alone and significantly enhanced OAS1B levels, suggesting an intracellular protein–protein interaction in bacterial cells.

Results

Analysis of the ATPase activity of ABCF3

ABCF3 protein was expressed from pET28a-*abcf3* (Fig. 1*A*) or pGEX-*abcf3* (Fig. 1*B*), as described under "Experimental procedures." These two clones produced ABCF3 with an N-terminal His-tag and GST-tag, respectively. A basal activity of 39 nmol/min/mg in 50 mM HEPES containing 125 mM NaCl, pH 7.5, was observed when the GST-tag was still present (Fig. 1, *B*

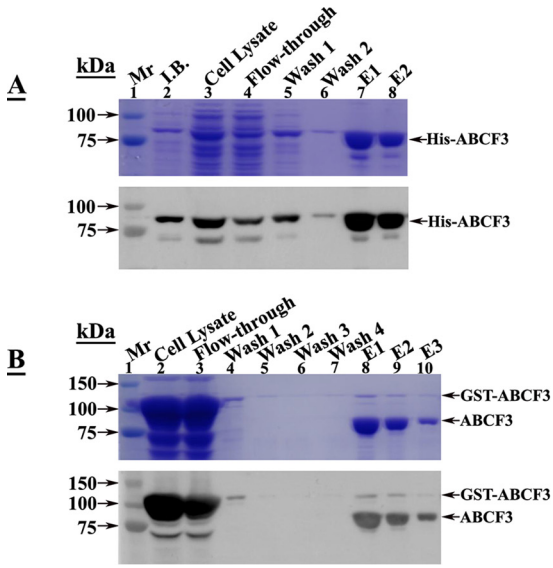

C

ATPase Activity of Purified ABCF3		
Protein	Yield (mg/ml)	ATPase Activity (nmole/min/mg)
GST-ABCF3	1.3	39 ± 12
ABCF3 (no GST Tag)	0.4	125 ± 6
His-ABCF3	1.3	132 ± 20

Figure 1. Expression and purification of ABCF3. Protein purification and ATPase activity assays were performed as described under "Experimental procedures." *A, E. coli* HMS174(DE3) cells containing pET28a-*abcf3* were used for purification of ABCF3. Samples 2–6 were normalized by volume. Equal volumes (10 μl) were then analyzed using 10% SDS-PAGE, followed by staining with Coomassie Blue and Western blot analysis using anti-ABCF3 (1:2000). Two μl of the 1-ml fractions were analyzed in *lanes 7* and *8*. *Lane 1, Mr* (marker); *lane 2,* inclusion body (I.B.); *lane 3,* cell lysate; *lane 4,* column flow-through; *lane 5,* washed with 50 ml of 30 mM imidazole in Buffer A (1× PBS, 20% glycerol, pH 7.4); *lane 6,* washed with 1 ml of 100 mM imidazole in Buffer A; *lanes 7* and *8*, 1 ml of the elution fractions, each with 200 mM imidazole in Buffer A. *B, E. coli* Rosetta 2(DE3)pLysS cells containing pGEX-*abcf3* were used for purification of ABCF3 with GST-tag cleavage during elution. Samples 2–7 were normalized by volume. Equal volumes (10 μl) were then analyzed using 10% SDS-PAGE, followed by staining with Coomassie Blue and Western blot analysis using anti-ABCF3 (1:2000). Two μl of a 1-ml elution were analyzed in *lanes 8–10*. *Lane 1, Mr*; *lane 2,* cell lysate; *lane 3,* column flow-through; *lanes 4–6*, washed with 10 ml of Buffer A each; *lane 7,* washed with 20 ml of Buffer B (1× cleavage buffer, 20% glycerol, pH 7.0); *lanes 8–10*, elution fractions 1–3 with 1 ml of Buffer B after GST tag cleavage with PreScission Protease (GE Healthcare). *C, table* shows the yield of purified ABCF3 and mean ± S.D. $n = 10$ experiments for 5 μg of basal ABCF3 ATPase activity. A Mann-Whitney test showed there was a significant difference between basal ATPase activity of GST–ABCF3 and ABCF3, p value 0.0022; between GST–ABCF3 and His–ABCF3, p value 0.0007; and there was no significant difference between ABCF3 and His–ABCF3 basal ATPase activities, p value 0.7546.

and *C*). In contrast, a basal activity of 125 nmol/min/mg was observed when the GST-tag was removed. His-tagged ABCF3 exhibited a basal ATPase activity of 132 nmol/min/mg that was similar to that of untagged ABCF3 (Fig. 1, *A* and *C*), indicating that the presence of the His-tag at the N terminus of ABCF3 had no deleterious effect on its activity. Also, the yield of pGEX*f3*-expressed ABCF3 protein obtained after removal of the GST tag was significantly lower than that of pET28a*f3*-expressed His–ABCF3 (Fig. 1, *A–C*). Purified His-tagged ABCF3 protein was used in the subsequent experiments.

Modulation of the ATPase activity of ABCF3 by potential ligands

The substrates of the ABCF3 protein are currently unknown. To identify potential ligands, the effect of various lipids, sterols, and drugs on the ATPase activity of ABCF3 was analyzed (Fig. 2, *A–J*, *gray diamond*) as described under "Experimental procedures." The selected lipids and drugs were chosen based on previous reports in the literature (11, 45–49). To remove background activity, the effect of each ligand on the activity of the double Walker A mutant K216A/K531A (described later) was also analyzed (Fig. 2, *A–J*, *tan circle*). The normalized activities were then calculated by subtracting the activity of the double mutant from the WT ABCF3 activity at each ligand concentration (Fig. 2, *black square*). The data in Fig. 2 show that the ATPase activity of ABCF3 was significantly modulated by sphingosine, sphingomyelin, platelet-activating factor (PAF), lysophosphatidylcholine (LPC), lysophosphatidylinositol (LPI), lyso-PAF, cholesterol, and alkyl ether lipids. Sphingosine, sphingomyelin, PAF, and LPC induced nearly a 3-fold enhancement in activity (Fig. 2, *A–D*). The alkyl ether lipid miltefosine induced a biphasic response with ATPase activity stimulated at low concentrations and inhibited at higher concentrations (Fig. 2*E*). In contrast, the other two alkyl lipids, edelfosine and perifosine, as well as LPI, lyso-PAF, and cholesterol, inhibited ATPase activity at all concentrations tested, including very low concentrations (Fig. 2, *F–J*). Several drugs, which are known to be substrates of multidrug resistance pumps, such as Hoechst 33342, verapamil, vinblastine, and quinidine as well as lipids, including phosphatidylcholine, phosphatidylethanolamine, sphingosine 1-phosphate, ceramide, and dihydroceramide, had no effect on the ATPase activity of ABCF3 (Fig. 2*K*).

Role of the two NBDs of ABCF3 in ATP binding

Similar to other class 2 ABC proteins, mouse ABCF3 contains two tandem NBDs connected by an 80-amino acid long linker sequence with each NBD containing all of the previously described conserved motifs (Fig. S1*A*). Alignment of the amino acid sequence of mouse ABCF3 with those of other class 2 eukaryotic and prokaryotic ABC proteins showed a very high degree of sequence similarity in all of the conserved motifs present in both NBD1 (Fig. S1*B*) and NBD2 (Fig. S1*C*). The human and mouse ABCF3 proteins showed more than 95% overall sequence identity with each other extending over the entire sequence of these proteins. The inter-ABC domain linker region of bacterial ABCF proteins contains conserved sequences and several charged residues (Fig. S2*A*) (21, 23, 40). An alignment of the bacterial and eukaryotic linker sequences

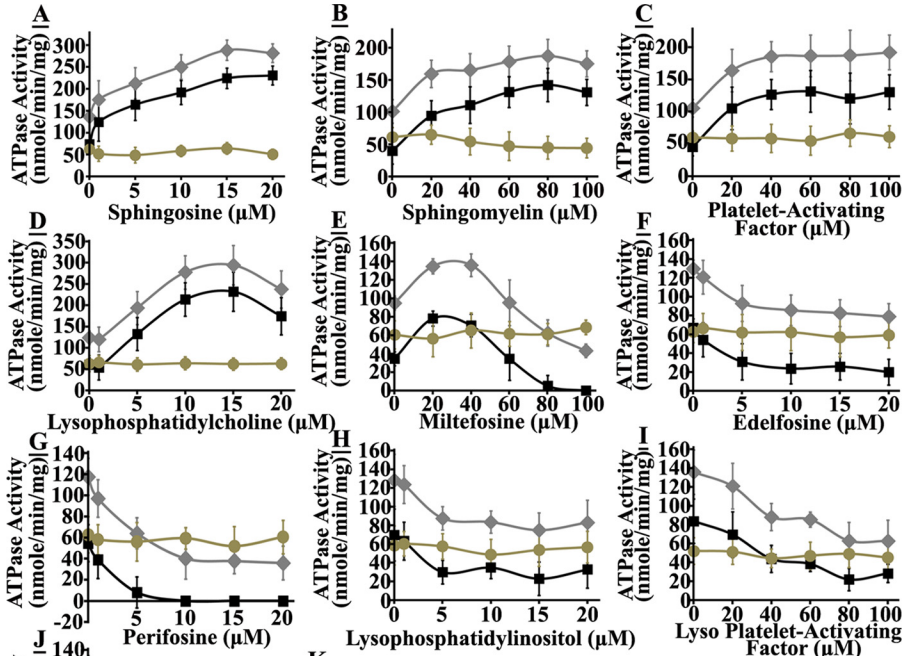

K

Effect of Potential Ligands on ABCF3 ATPase Activity	
MDR Drugs	**Fold Change**
Hoechst 33342	No Effect
Quinidine	No Effect
Verapamil	No Effect
Vinblastine	No Effect
Lipids, Sterol	**Fold Change**
Sphingosine	2.92 (15μM**)
Sphingosine-1-Phosphate	No Effect
Sphingomyelin	3.08 (100μM*)
Ceramide	No Effect
Dihydroceramide	No Effect
Platelet-activating factor	2.80 (40μM*)
Lyso Platelet-activating factor	0.26 (80μM*)
10:0 Phosphatidylcholine	No Effect
14:0 Phosphatidylethanolamine	No Effect
Lysophosphatidylcholine	3.83 (15μM***)
Lysophosphatidylinositol	0.33 (15μM***)
Cholesterol	0.32 (80μM*)
Alkyl Ether Lipids	**Fold Change**
Miltefosine	2.05 (40μM*) ; 0.15 (80μM*)
Edelfosine	0.30 (20μM**)
Perifosine	0.13 (5μM*)

Figure 2. Modulation of the ATPase activity of purified ABCF3 by ligands. *A–J,* increasing concentrations of sphingosine (*A*), sphingomyelin (*B*), platelet-activating factor (*C*), lysophosphatidylcholine (*D*), miltefosine (*E*), edelfosine (*F*), perifosine (*G*), lysophosphatidylinositol (*H*), lyso platelet–activating factor (*I*), and cholesterol (*J*) were added to 5 μg of purified ABCF3 in a 1-ml volume reaction. The coupled assay for ATPase activity was carried out as described under "Experimental procedures." Data points represent mean ATPase activity with standard deviation for 10 trials in nanomoles/min/mg. *Gray diamond* indicates WT ABCF3; *tan circle* indicates K216A/K531A mutant ABCF3; and *black square* indicates normalized WT ABCF3 ATPase activities. ATPase activities were normalized by subtracting the activity of K216A/K531A mutant protein from WT ABCF3 activity at each ligand concentration. *K, table* shows a summary of fold-change in ATPase activity produced by various ligands. The activity in the absence of a ligand was designated as 1.0. Fold-change of >1 implies stimulation, and <1 implies inhibition. The reported fold-change was observed at the concentration indicated in *parentheses*. The results of Wilcoxon matched-pairs signed rank tests comparing normalized basal ATPase activity and normalized ligand-stimulated activity of WT ABCF3 are shown next to the ligand concentration values. ***, p value ≤ 0.001; **, p value ≤ 0.01; *, p value ≤ 0.05.

showed regions of relatively high homology between the two groups (marked with *green highlighted boxes*, Fig. S2*B*) and within members of the eukaryotic group (Fig. S2*C*), suggesting that the linker region of eukaryotic proteins may also play an important role in the function of these proteins.

To determine the function of each NBD of the mouse ABCF3 protein, point mutations were made in either the conserved lysine in the Walker A motif that is known to be critical for ATP binding or in the conserved glutamate in the Walker B motif that plays an important role in ATP hydrolysis (12, 14). Clones containing simultaneous mutations in both NBDs of ABCF3 were also made. The nucleotide-binding characteristics of the purified WT and mutated ABCF3 proteins were initially analyzed by intrinsic tryptophan (Trp) fluorescence quenching. This approach is commonly used to determine conformational changes in proteins in response to the binding of nucleotides and other substrates (42). An emission scan of ABCF3 and NATA (a tryptophan analog) showed that, as expected, the environment of the Trp residues in ABCF3 is more nonpolar than that of NATA (Fig. S3*A*). Titration of purified ABCF3 protein with ATP or ADP showed saturable quenching, indicating specific binding of each nucleotide (Fig. S3*B*). However,

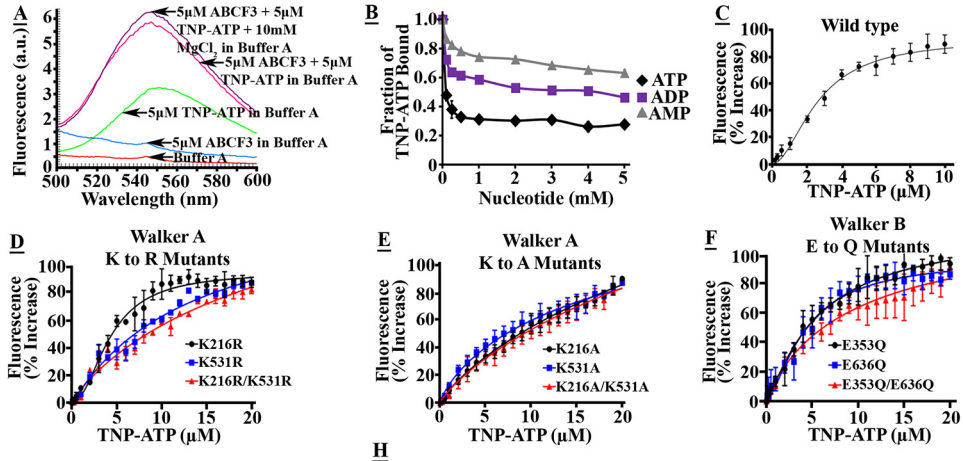

H

Kinetics of TNP-ATP binding to ABCF3		
Sample	$K_{0.5}$ (μM)	nH
Wild-type ABCF3	2.6 ± 0.1 μM	1.8 ± 0.1
K216R (NBD1)	4.2 ± 0.2 μM	2.0 ± 0.2
K531R (NBD2)	13.4 ± 3.9 μM	1.0 ± 0.1
K216R/K531R (NBD1/NBD2)	28.4 ± 21.4 μM	0.9 ± 0.1
K216A (NBD1)	52.7 ± 38.0 μM	0.8 ± 0.1
K531A (NBD2)	22.1 ± 12.1 μM	0.9 ± 0.1
K216A/K531A (NBD1/NBD2)	58.6 ± 66.9 μM	0.8 ± 0.1
E353Q (NBD1)	5.7 ± 0.9 μM	1.2 ± 0.1
E636Q (NBD2)	4.2 ± 0.4 μM	1.5 ± 0.2
E353Q/E636Q (NBD1/NBD2)	9.9 ± 4.5 μM	0.9 ± 0.1
E353A (NBD1)	12.5 ± 1.4 μM	1.0 ± 0.0
E636A (NBD2)	5.9 ± 0.5 μM	1.3 ± 0.1
E353A/E636A (NBD1/NBD2)	8.9 ± 2.1 μM	1.0 ± 0.1

Figure 3. Binding of TNP-ATP to WT ABCF3 or mutated proteins. *A,* fluorescence emission of TNP-ATP bound to ABCF3. The fluorescence emission spectrum of 5 μM TNP-ATP in Buffer A (1 × PBS, 20% glycerol, pH 7.4) was examined in the presence or absence of 5 μM ABCF3. Excitation occurred at 403 nm, and emission was recorded between 450 and 600 nm. Scans carried out in the presence or absence of TNP-ATP and ABCF3 are shown. *B,* displacement of TNP-ATP by ATP, ADP, or AMP. Different concentrations of ATP (*black diamond*), ADP (*purple square*), or AMP (*gray triangle*) were added to a 500 μl solution containing 5 μM ABCF3 with 5 μM TNP-ATP and 10 mM $MgCl_2$ after an incubation period of 5 min at room temperature. Fluorescence values were obtained after each addition of nucleotide and corrected as described. The initial fluorescence (before addition of nucleotides) was set as 1.0, and the fraction of TNP-ATP bound to ABCF3 after addition of nucleotides was calculated. Each plotted value represents the average of four trials, and where not visible the standard deviation lies within the data points. *C,* kinetic analysis of TNP-ATP binding to purified WT ABCF3. Titrations of ABCF3 with increasing concentrations of TNP-ATP were carried out. Aliquots of TNP-ATP were added to a 500 μl solution of 5 μM ABCF3 in Buffer A, and the fluorescence intensity (403 nm excitation, 450–600 nm emission) was recorded after each addition. Blank titrations with each TNP-ATP concentration (without addition of ABCF3) were also carried out. Fluorescence values were corrected as described under "Experimental procedures" and plotted using GraphPad Prism. *D–G,* kinetic analysis of TNP-ATP binding to mutated proteins. *D,* Walker A lysine to arginine mutations NBD1 (*black circle*); NBD2 (*blue square*); and double NBD1/NBD2 (*red triangle*). *E,* Walker A lysine to alanine. *F,* Walker B glutamic acid to glutamine. *G,* Walker B glutamic acid to alanine. Each data point represents the average of four trials. Where not visible the standard deviation lies within the data points. *H,* summary of TNP-ATP binding kinetics to WT and Walker A and B mutants fitted to allosteric sigmoidal binding model. Nonconservative mutations are shown in *red font*. The standard deviations are provided for each. *nH* = Hill coefficient.

the corrected fluorescence data could be fitted to single-site Michaelis-Menten kinetics suggesting that there is only one nucleotide-binding site in WT ABCF3 (Fig. S3*B*). This may be due to the asymmetric distribution of the Trp residues in ABCF3 (with four located in NBD1 and only one near NBD2, see Fig. S1*A*), which likely introduces a bias in the Trp-quenching experiments. Analysis of single or double Walker A mutants (K216R, K531R, or K216R/K531R) surprisingly showed that the ATP-binding affinity of each of these mutants was unaffected compared with that of WT ABCF3 (Fig. S3*C*), further indicating that Trp-quenching analysis may not be suitable for studying nucleotide binding to ABCF3.

To further investigate nucleotide binding, TNP-ATP, a fluorescent analog of ATP, was used. TNP-ATP alone exhibits some fluorescence in solution; however, its interaction with the nucleotide-binding pocket of a protein results in enhanced fluorescence (44, 55–57). TNP-ATP binding to ABCF3 resulted in a 2-fold increase in fluorescence (in the presence or absence of 10 mM $MgCl_2$) compared with TNP-ATP in buffer (Fig. 3*A*). Moreover, a red shift in λ_{max} from 551 to 545 nm was also observed indicating that TNP-ATP binding occurs within a hydrophobic region in ABCF3. To determine whether TNP-ATP binds to the ATP-binding pocket(s), increasing concentrations of different nucleotides, including ATP, ADP, or AMP, were added to TNP-ATP–bound ABCF3. It was expected that the addition of nucleotides would displace TNP-ATP from the binding pocket and result in a decrease in fluorescence, as reported previously (44, 55–57). The addition of 0.1 mM ATP resulted in a sharp decrease in fluorescence indicating displacement of TNP-ATP (Fig. 3*B*). Significantly less displacement was seen with either 0.1 mM ADP or AMP. These results suggest that TNP-ATP binds specifically to the nucleotide-binding pocket(s) in ABCF3 and that ATP binds with higher affinity than either ADP or AMP.

To determine the ABCF3 binding affinity for TNP-ATP, 5 μM ABCF3 was titrated with increasing concentrations of TNP-ATP ranging between 0.1 and 20 μM. TNP-ATP binding to WT ABCF3 followed sigmoidal kinetics, suggesting the presence of two nucleotide-binding sites in this protein (Fig. 3*C*). The data could be fitted to an allosteric binding model that exhibited a

$K_{0.5}$ of less than 3 μM and a Hill coefficient of 1.8 (Fig. 3*H*), suggesting positive cooperativity between the two binding sites. To determine the effect of Walker A mutations on TNP-ATP binding, titrations were also carried out with the single (NBD1 or NBD2) and double (NBD1/NBD2) mutant ABCF3 proteins. Lysine to arginine substitution mutations in the Walker A motif in each NBD of ABCF3 (K216R or K531R) resulted in higher $K_{0.5}$ values, implying a lower-binding affinity for TNP-ATP, as expected (Fig. 3, *D* and *H*). The K216R (NBD1) mutant protein bound TNP-ATP with a 2-fold higher $K_{0.5}$ than WT ABCF3, whereas the K531R (NBD2) mutant protein showed about a 5-fold higher $K_{0.5}$ (Fig. 3, *D* and *H*). The double mutant K216R/K531R protein exhibited the highest $K_{0.5}$, which was almost 10-fold higher than that of the WT protein. These data suggest that both NBDs in ABCF3 contribute to ATP binding, but NBD2 plays a more important role. Interestingly, the NBD2 mutant K531R protein provided the best fit with the single-site Michaelis-Menten model and showed a Hill coefficient of 1.0, which differed from the Hill coefficient of 1.8 observed for the WT protein. The NBD1 mutant K216R protein, however, still displayed allosteric binding of TNP-ATP with a Hill coefficient of 2.0. Together, these results suggest that TNP-ATP still binds to the mutated NBD1 site (K216R) albeit with a 2-fold lower affinity, but TNP-ATP binding to the mutated NBD2 (K531R) is significantly negatively impacted.

Since the conservative lysine to arginine mutations described above resulted in only limited loss of function of ABCF3 (especially for the NBD1 K216R mutant), nonconservative mutations of lysine to alanine were also constructed to further examine the role of each NBD. As expected, these mutations (K216A, K531A, and K216A/K531A) produced a much more drastic effect on TNP-ATP binding resulting in incomplete saturation when each protein was titrated with increasing concentrations of TNP-ATP (Fig. 3*E*). Moreover, the $K_{0.5}$ value in each case was significantly higher as compared with the lysine to arginine mutations, and the Hill coefficient in each case was $<$1.0 (Fig. 3*H*, shown in *red font*). The combination of the nonsaturating binding curves seen in Fig. 3*E* and the high error in $K_{0.5}$ values reported by GraphPad in Fig. 3*H* suggested that these $K_{0.5}$ values are most likely underestimated. Overall, these results imply that TNP-ATP binding activity is severely compromised in proteins with the nonconservative lysine to alanine mutations in either NBD and confirm a role for each NBD of ABCF3 in ATP binding.

Although the Walker B motif of ABC proteins plays an important role in ATP hydrolysis (described below), the effect of single (E353Q or E636Q) and double (E353Q/E636Q) point mutations in Walker B on TNP-ATP binding was also investigated (Fig. 3*F*). As expected, the effect of conservative Walker B mutations on TNP-ATP binding was less severe than that observed for the conservative Walker A mutations. These three mutants displayed a slightly enhanced $K_{0.5}$, with the double mutant showing the largest increase (Fig. 3*H*). Nonconservative Walker B mutations (E353A, E636A, and E353A/E636A) were also examined for their effect on TNP-ATP binding. The effect of these mutations was also not as severe as that observed with the nonconservative Walker A mutations (Fig. 3, *G* and *H*).

Role of the two NBDs of ABCF3 in ATP hydrolysis

The effect of the Walker A mutations (K216R, K531R, K216A, and K531A) or the Walker B mutations (E353Q, E636Q, E353A, and E636A) on ATPase activity was next determined. The most drastic effect on basal activity was observed for the single nonconservative point mutation, K216A, in NBD1, which resulted in less than 30% residual activity (Fig. 4*A*, *column 1,* highlighted in *red font*). In contrast, a protein with the single K531A mutation in NBD2 retained 100% of the basal activity, whereas the double mutation K216A/K531A showed less than 30% activity similar to K216A (Fig. 4*A*, *column 1*). ABCF3 proteins containing conserved double Walker A (Lys to Arg) or Walker B (Glu to Gln) mutations retained about 60–70% residual activity. The double Walker B (nonconservative Glu to Ala) mutant protein, however, showed normal basal activity for unexplained reasons (Fig. 4*A*, *column 1,* highlighted in *red font*). Because the basal activity does not represent specific ligand-stimulated activity, the finding that the effect of various point mutations on basal activity varied is not surprising.

The ATPase activity of WT ABCF3 was previously shown to be stimulated by sphingosine (Fig. 2*A*), and the effect of sphingosine on the activities of the Walker A and Walker B mutant proteins was next determined. The NBD1 and NBD2 mutant proteins behaved differently after addition of sphingosine. Although the ATPase activity of WT ABCF3 was stimulated about 3-fold by sphingosine, the activity of the NBD1 mutant K216A was stimulated 15-fold compared with its reduced basal activity (Fig. 4*A*, compare *columns 1* and *3*). The overall stimulated activity of K216A (626 nmol/min/mg) was 1.7-fold higher than the stimulated WT protein activity (367 nmol/min/mg). In contrast, the activity of the corresponding NBD2 K531A mutant protein was inhibited 3-fold by sphingosine, and the activity of the double K216A/K531A mutant protein was unaffected (Fig. 4*A*, *columns 1* and *3*). The protein with the conservative Walker A mutation K216R in NBD1 also showed about a 3-fold stimulation of activity, whereas the K531R NBD2 mutant protein showed a 2-fold decrease (Fig. 4*A*, *columns 1* and *3*). The Walker B NBD1 mutant proteins (E353A and E353Q) also showed a 4–6-fold stimulation in activity, whereas the activities of the NBD2 mutant proteins (E636A and E636Q) were decreased by about 1.5-fold, overall indicating a similar trend for the NBD1 and NBD2 mutations. Since the nonconservative double Walker A mutation K216A/K531A was most detrimental to the basal (Fig. 4*A*, *column 1*) and sphingosine-stimulated (*column 3*) ATPase activities, the residual activity of this mutant likely represents background or nonspecific activity. Therefore, the ATPase activity data were normalized by subtracting the basal and stimulated activity of the double mutant from the corresponding activities of WT ABCF3 and all other mutants (Fig. 4*A*, *columns 2* and *4*). A scatter plot of the normalized basal and sphingosine-stimulated ATPase activities of the WT and mutants is shown in Fig. 4*B*. After normalization, the ATPase activity trends remained the same. The activity of the different NBD1 mutants was stimulated by sphingosine, and the activity of different NBD2 mutants was inhibited, although the degree of fold-stimulation or inhibition was

A

Effect of Walker A and Walker B Mutations on ABCF3 ATPase Activity (nmole/min/mg)				
Column	1	2	3	4
Sample	Basal	Normalized Basal	+Sphingosine	Normalized + Sphingosine
WT ABCF3	129 ± 14	92 ± 16	367 ± 77	295 ± 66 ****
K216R (NBD1)	158 ± 19	116 ± 19 *	416 ± 68	376 ± 68 **
K531R (NBD2)	160 ± 22	117 ± 22 *	79 ± 16	35 ± 23 **
K216R/K531R (NBD1/NBD2)	74 ± 12	40 ± 19 **	55 ± 8	13 ± 9 **
K216A (NBD1)	40 ± 8	2 ± 3 ***	626 ± 88	586 ± 88 **
K531A (NBD2)	135 ± 19	101 ± 31	44 ± 23	14 ± 14 **
K216A/K531A (NBD1/NBD2)	43 ± 8	–	40 ± 8	–
E353Q (NBD1)	77 ± 17	34 ± 16 ***	452 ± 78	412 ± 78 ***
E636Q (NBD2)	75 ± 14	36 ± 15 ****	49 ± 12	11 ± 13 **
E353Q/E636Q (NBD1/NBD2)	91 ± 20	46 ± 21 **	73 ± 18	22 ± 20 *
E353A (NBD1)	155 ± 23	112 ± 23 *	661 ± 143	621 ± 143 ***
E636A (NBD2)	69 ± 14	21 ± 16 **	52 ± 11	2 ± 6 **
E353A/E636A (NBD1/NBD2)	153 ± 15	110 ± 12 **	97 ± 17	56 ± 16 **

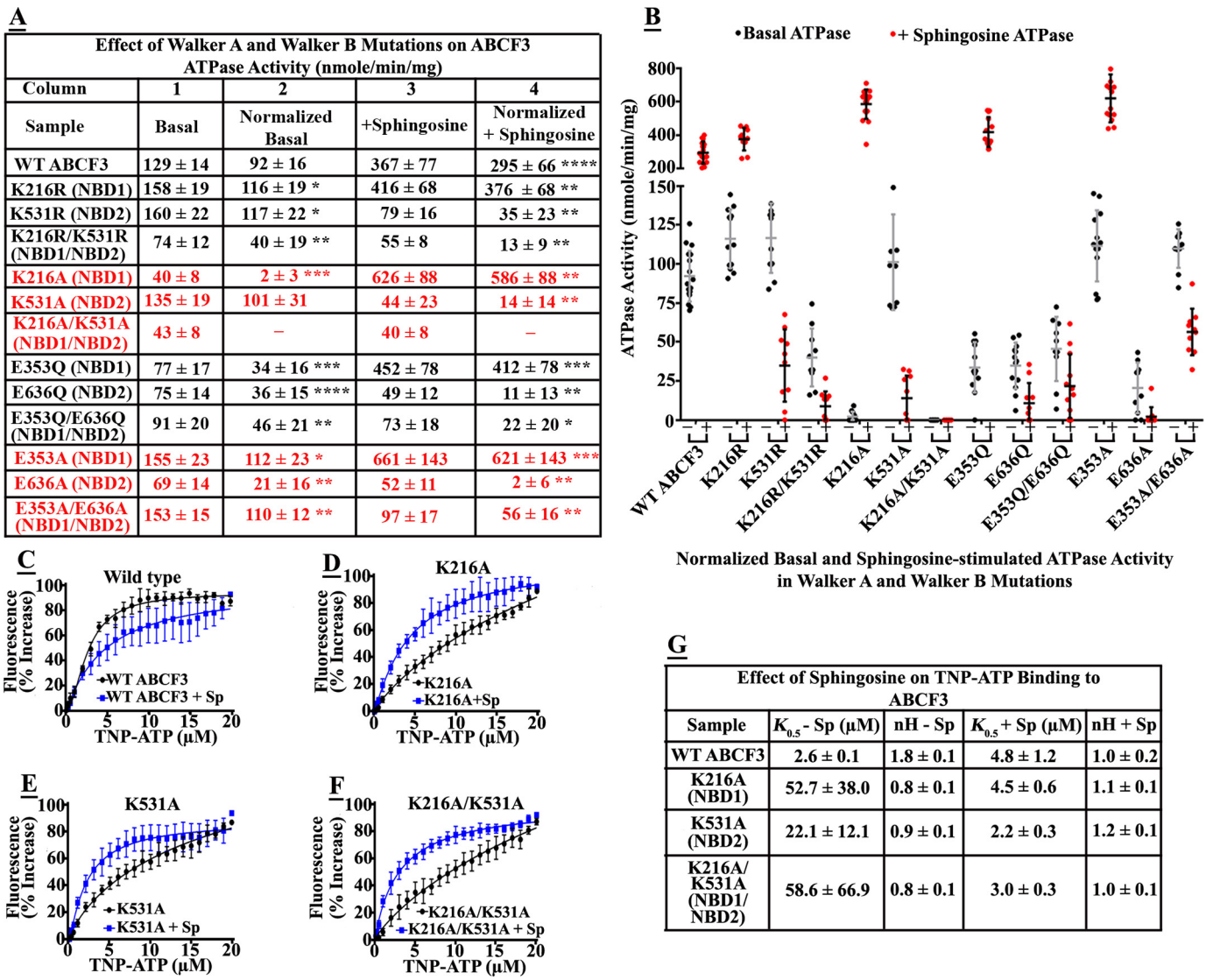

G

Effect of Sphingosine on TNP-ATP Binding to ABCF3				
Sample	$K_{0.5}$ - Sp (μM)	nH - Sp	$K_{0.5}$ + Sp (μM)	nH + Sp
WT ABCF3	2.6 ± 0.1	1.8 ± 0.1	4.8 ± 1.2	1.0 ± 0.2
K216A (NBD1)	52.7 ± 38.0	0.8 ± 0.1	4.5 ± 0.6	1.1 ± 0.1
K531A (NBD2)	22.1 ± 12.1	0.9 ± 0.1	2.2 ± 0.3	1.2 ± 0.1
K216A/K531A (NBD1/NBD2)	58.6 ± 66.9	0.8 ± 0.1	3.0 ± 0.3	1.0 ± 0.1

Figure 4. Effect of Walker A or Walker B mutations on ATP hydrolysis and TNP-ATP binding in the presence of 15 μM sphingosine. *A, table* summarizes the basal and sphingosine-stimulated ATPase activities in nanomoles/min/mg of purified WT ABCF3 or the Walker A and Walker B mutated proteins. Same amount of purified ABCF3 protein (5 μg) was used in each assay, and the data were normalized by subtracting the basal or sphingosine stimulated activity of K216A/K531A from WT and Walker A and Walker B mutant protein activities. The data represent the mean of at least 10 trials with the standard deviation provided. Nonconservative mutations are shown in *red font*. The results of Wilcoxon matched-pairs signed rank tests comparing normalized basal ATPase activity of WT to Walker A or B mutated proteins are shown with *asterisks* in *column 2*. The results of Wilcoxon matched-pairs signed rank tests comparing normalized basal to normalized sphingosine-stimulated ATPase activity for each protein sample are shown with *asterisks* in *column 4*. ****, *p* value ≤0.0001; ***, *p* value ≤0.001; **, *p* value ≤0.01; *, *p* value ≤0.05. *B,* scatter plot showing the normalized basal (*black circle,* −) and sphingosine-stimulated (*red circle,* +) ATPase activities in nanomoles/min/mg of Walker A and B mutant proteins. − (*black*) and + (*red*) indicate the absence or presence of sphingosine, respectively. *C–F,* kinetic analysis of TNP-ATP binding to WT ABCF3 or Walker A lysine to alanine mutated proteins with (*blue square*) or without (*black circle*) 15 μM sphingosine. *C,* WT protein. *D,* NBD1 mutant K216A protein. *E,* NBD2 mutant K531A protein. *F,* NBD1/NBD2 double mutant K216A/K531A protein. The plotted values represent the average of four trials fitted to an allosteric sigmoidal model using GraphPad Prism software. *G,* summary of TNP-ATP binding kinetics to WT and mutated proteins fitted to an allosteric sigmoidal binding model. Sp = sphingosine.

altered to varying degrees for the different mutant proteins. For example, the normalized activity of the K216A mutant protein with sphingosine was on average nearly 300-fold higher compared with its basal activity (Fig. 4*A*, *column 4*). This is due to the raw basal activities of the K216A and K216A/K531A mutants being very similar, as stated above, and thus after normalization K216A exhibited minimal basal activity (Fig. 4*A*, *column 2*), resulting in a much higher fold-change of stimulated activity with a broader range (164–337) as shown in Fig. 5.

To determine whether sphingosine enhances the catalytic activity of the NBD1 mutant K216A by increasing its affinity for ATP, 5 μM purified WT or K216A protein was titrated with increasing concentrations of TNP-ATP in the presence of 15 μM sphingosine. While the addition of sphingosine did not produce a significant change in the binding affinity of WT ABCF3 for TNP-ATP (Fig. 4*C*), the saturation curve no longer exhibited sigmoidal behavior, and the kinetics yielded a Hill coefficient of 1.0 instead of 1.8 seen in the absence of sphingosine (Fig. 4*G*). As predicted, the binding affinity of the NBD1 mutant K216A for TNP-ATP was significantly enhanced by the presence of sphingosine (Fig. 4, *D* and *G*). Moreover, the binding kinetics of the K216A mutant exhibited saturable binding, which is in contrast to the incomplete saturation seen in the absence of the ligand (Fig. 4*D*). The $K_{0.5}$ for K216A in the pres-

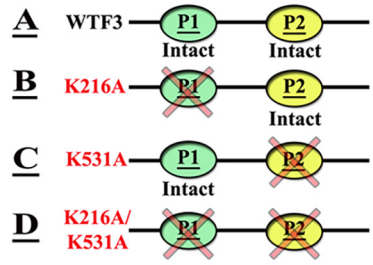

	Normalized ATPase Activity		TNP-ATP Binding			
	1	2	3	4	5	6
	Basal (relative to WT)	+ Sphingosine (relative to Basal)	$K_{0.5}$ Basal (Relative to WT)	$K_{0.5}$ + Sphingosine (Relative to WT)	nH Basal	nH +Sphingosine
A	1.0	≈ 1.81-4.14	1.0	1.0	1.8	1.0
B	0.02	≈ 164-337	≈ 20	1.0	0.8	1.1
C	1.10	≈ 0.04-0.42	≈ 9	0.5	0.9	1.2
D	0.0	0.0	≈ 23	0.6	0.8	1.0

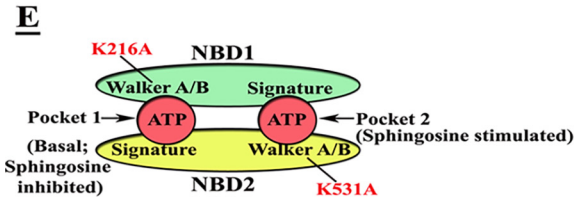

Figure 5. Proposed model for the function of two ATP-binding pockets in ABCF3. *A–D,* linear schematic of WT ABCF3 and proteins mutated in the Walker A motif (K216A, K531A, and K216A/K531A), each showing the two ATP-binding pockets *P1* and *P2*. The mutated sites are marked with ×. The ATPase activity and the TNP-ATP– binding data for WT and mutants are summarized in the *table*. The normalized activities shown in Fig. 4*A* were used to generate the relative ATPase activity values in *columns 1* and *2*. In *column 1*, the WT normalized basal ATPase values were designated as 1.0, and the relative ATPase values for each ABCF3 mutant were calculated. In *column 2*, the fold-change was calculated by dividing the normalized sphingosine-stimulated activity of the WT and mutant ABCF3 proteins by the normalized basal activity of each protein. The range indicates variability, calculated from 10 individual experiments. Values of >1.0 indicate stimulation. Values of <1.0 indicate inhibition, with a lower value indicating greater inhibition. *Columns 3–6* are based on TNP-ATP binding analyses shown in Fig. 4, *C–G*. For *column 3*, the WT $K_{0.5}$ value without sphingosine was designated as 1.0, and the relative $K_{0.5}$ values for each mutant without sphingosine are shown. In *column 4*, WT ABCF3 $K_{0.5}$ values with 15 μM sphingosine were designated as 1.0, and the relative $K_{0.5}$ values with sphingosine for each mutant are shown. *Column 5* displays the Hill coefficient (*nH*) for WT and mutant ABCF3 with TNP-ATP only, and *column 6* shows *nH* values for WT and mutant ABCF3 with TNP-ATP in the presence of 15 μM sphingosine. *E,* model of the head–to–tail interaction between the NBD1 and NBD2 domains of ABCF3 that result in the formation of two ATP-binding pockets at their interface. The locations of the NBD1 mutant K216A and NBD2 mutant K531A are indicated (*red*). Based on the data provided in the *table*, pockets 1 and 2 are proposed to be the sites for basal and sphingosine-stimulated ATPase activity, respectively. The function of pocket 1 is proposed to be inhibited by sphingosine simultaneously when pocket 2 is stimulated.

ence of sphingosine was about 10-fold lower than that seen in the absence of sphingosine and was now in the same range as for WT ABCF3. Despite the very high binding affinity, the binding curves were not sigmoidal, and the kinetic data showed a Hill coefficient of 1.1 (Fig. 4*G*). Surprisingly, addition of sphingosine also resulted in saturable binding of TNP-ATP to the NBD2 mutant K531A and the double mutant K216A/K531A with significantly reduced $K_{0.5}$ values (Fig. 4, *E–G*), even though the ATPase activities of these mutants were not stimulated by sphingosine (Fig. 4, *A* and *B*).

The two ATP-binding pockets in WT ABCF3 protein are shown as P1 and P2 in the linear schematic shown in Fig. 5*A*, and the negative effect of point mutations on pocket function is indicated in Fig. 5, *B–D*. The accompanying *table* in Fig. 5 summarizes the differential effects of NBD1 and NBD2 mutations on TNP-ATP binding and the ATPase activities shown in Fig. 4. Based on the data shown in Figs. 4 and 5, *A–D*, a model of the function of each pocket was generated (Fig. 5*E*). The ATP-binding pockets are expected to be located at the interface of NBD1 and NBD2 in ABCF3 and to be formed by a head–to–tail interaction previously seen in other ABC proteins (12). Pocket 1 (P1) is formed by association of Walker A and Walker B regions of NBD1 with the signature motif of NBD2, whereas pocket 2 (P2) contains the opposite arrangement. The possible implications of this model for the catalytic mechanism of ABCF3 are discussed later.

Co-expression of OAS1B and ABCF3 in bacteria

OAS1B protein was previously shown to be localized to the ER membrane in mammalian cells (9). This is proposed to result from the presence of a putative TM domain located at the C terminus of OAS1B (9). As bacteria contain only a cell membrane and lack organelle membranes, we hypothesized that an ABCF3–OAS1B complex formed in bacterial cells might localize to the cell membrane and provide a model for studying function, including lipid transport, by this complex. Co-expression of OAS1B and ABCF3 was analyzed in *Escherichia coli* cells. The expression of full-length *oas1b* alone from pGEX-*oas1b* at 20 °C resulted in complete growth arrest within 30 min of induction of protein expression in *E. coli* cells; however, expression of the truncated OAS1B protein lacking the putative TM domain (from pGEX-*oas1bΔtm*) induced no growth inhibition (Fig. 6*A*). Western blot analysis showed significantly higher levels of the OAS1BΔTM protein compared with the full-length OAS1B (Fig. 6*B*, compare *lanes 2–4* with *lanes 5–7*). This result was expected because samples used in Fig. 6*B*, *lanes 2–4,* were derived from viable cells, whereas samples in *lanes 5–7* were derived from growth-inhibited cells. Overall, the differential growth effect observed was attributed to the presence of a TMD on the full-length OAS1B protein. Most of the OAS1BΔTM protein was sequestered in the inclusion body (IB) fraction (Fig.

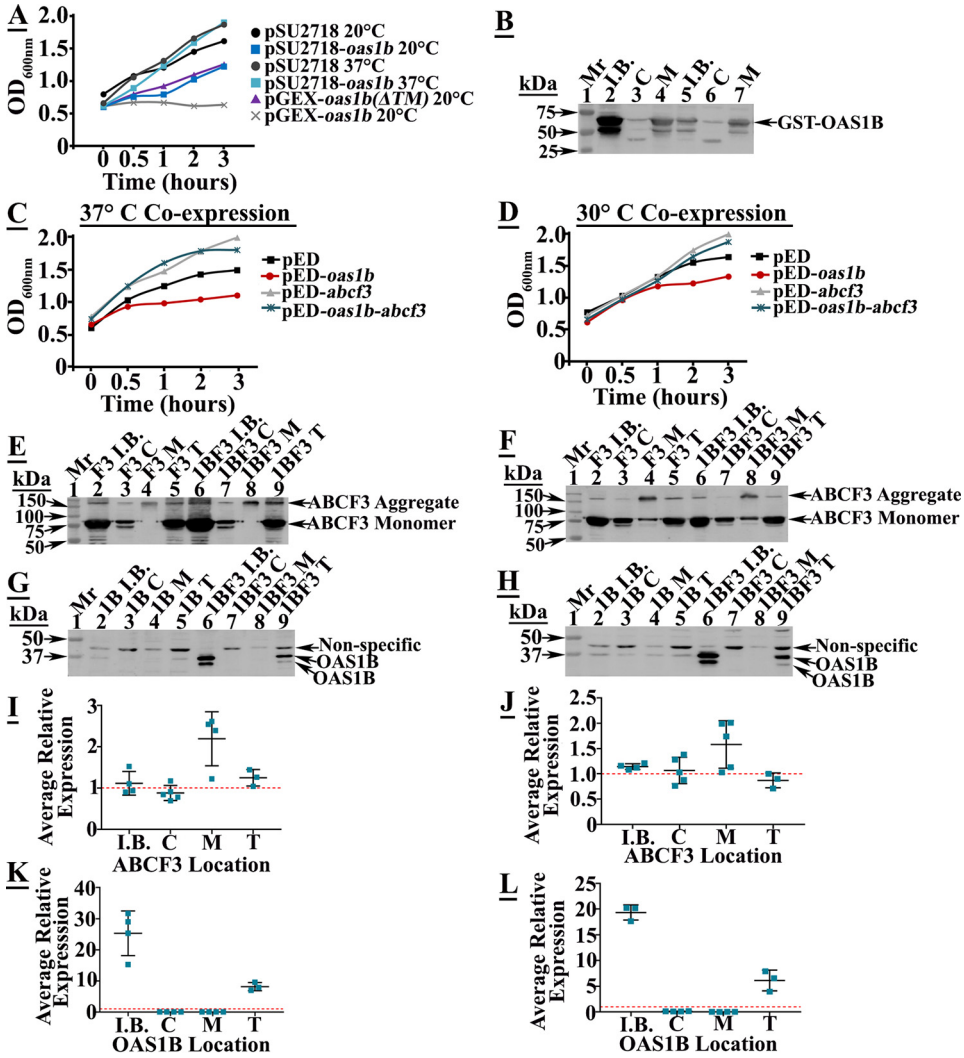

Figure 6. Co-expression of *oas1b* and *abcf3* in bacteria. *A* and *B,* effect of expression of full-length OAS1B on growth of *E. coli* cells. *A,* Rosetta 2(DE3)pLysS cells containing pGEX-*oas1b* (*gray times sign*) or pGEX-*oas1b*(Δ*tm*) (*purple triangle*) or BL21 cells containing pSU2718 (*black circle*) or pSU2718-*oas1b* (*blue square*) were grown at 37 °C to mid-log phase ($A_{600\ nm}$ = 0.6) and induced with 0.25 mM IPTG for 3 h at 20 °C. BL21 cells containing pSU2718 (*dark gray circle*) or pSU2718-*oas1b* (*cyan square*) were also separately induced with 0.25 mM IPTG for 3 h at 37 °C. Cell growth was monitored for 3 h after induction. A representative growth experiment is shown. *B,* Western blot analysis using anti-OAS1 antibodies. pGEX-*oas1b*(Δ*tm*) or pGEX-*oas1b*– containing cells collected at the 3-h time point in *A* were fractionated as described to obtain the inclusion body (*I.B.*), cytosol (*C*), and membrane (*M*) fractions. Twenty five μg of each sample was loaded on 10% SDS-polyacrylamide gels, followed by Western blotting against anti-OAS1 (1:500) antibodies as described under "Experimental procedures." *Lane 1,* marker (*Mr*); *lanes 2–4*, OAS1B(ΔTM); *lanes 5–7*, OAS1B. *C* and *D,* effect of co-expression of OAS1B and ABCF3 on growth. *E. coli* Rosetta 2(DE3)pLysS cells containing pED (*black square*), pED-*oas1b* (*red circle*), pED-*abcf3* (*gray triangle*), or pED-*oas1b-abcf3* (*teal times sign*) were grown at 37 °C to mid-log phase ($A_{600\ nm}$ = 0.6) and induced with 0.25 mM IPTG for 3 h at 37 °C (*C*) or 30 °C (*D*). The growth was monitored at $A_{600\ nm}$ for 3 h after induction, and a representative growth experiment is shown. *E–H,* Western blot analysis of the levels of ABCF3 and OAS1B in cell fractions at 37 °C (*left panels*) or 30 °C (*right panels*). Samples collected at the 3-h time point in *C* and *D* were fractionated to obtain the inclusion body (*I.B.*), cytosol (*C*), and membrane (*M*) fractions. *T*, total sample. Samples were loaded on 10% SDS-polyacrylamide gels, followed by Western blotting with anti-ABCF3 (1:2000) or anti-OAS1 (1:500) antibodies. *E* and *F,* Western blot analysis using anti-ABCF3. Fifty μg of proteins were loaded with the exception of the *I.B.* samples where 25 μg of proteins were loaded. *Lane 1,* marker (*Mr*); *lanes 2–5*, ABCF3; *lanes 6–9*, OAS1B/ABCF3. *G* and *H,* Western blot analysis using anti-OAS1. Fifty μg of proteins were loaded in each lane, as described above for *E* and *F*. *Lane 1,* marker (*Mr*); *lanes 2–5*, OAS1B; *lanes 6–9*, OAS1B/ABCF3. *I–L*, scatter plots showing average relative expression of ABCF3 (*I* and *J*) and OAS1B (*K* and *L*) at 37 °C (*left panels*) or 30 °C (*right panels*). For comparison of protein levels in single and co-expression experiments, samples from all trials were electrophoresed together on the same gel and analyzed by densitometric scanning using Multi-Gauge version 2.3 software to obtain intensity values. The protein level obtained under the single expression condition in each case was designated as 1.0, which is shown as a *dotted red line* in the scatter plots for comparison with co-expression samples. Average intensity values obtained from ≥3 trials were then plotted. *1B* = OAS1B; *F3* = ABCF3; *1BF3* = OAS1B/ABCF3.

6*B*, *lane 2*), a phenomenon commonly seen when a heterologous protein is overexpressed in *E. coli* (58, 59).

The growth inhibitory effect of full-length OAS1B was also analyzed in two other bacterial expression systems. When full-length OAS1B was expressed at 20 °C from the extremely low-expression, pACYC-based, pSU2718 vector (60), growth inhibition was initially seen, but the cells were recovered after about 1 h of induction (Fig. 6*A*). Expression from pSU2718-*oas1b* at 37 °C, however, resulted in no growth inhibition (Fig. 6*A*). In contrast, expression of full-length OAS1B from the higher copy number pED-*oas1b* clone at 37 °C resulted in severe growth inhibition that was not reversed until 3 h (Fig. 6*C*). Growth inhibition, although to a lesser extent, was also seen when OAS1B was expressed at 30 °C (Fig. 6*D*). Expression of ABCF3 alone did not have a negative effect on bacterial growth under all tested conditions (Fig. 6, *C* and *D*).

To determine whether co-expression of *abcf3* would impact the growth inhibitory phenotype of *oas1b* expression, the growth of *E. coli* transformed with the pED clones expressing *abcf3* (pED-*abcf3*), *oas1b* (pED-*oas1b*), or both *abcf3* and *oas1b* (pED-*oas1b-abcf3*) genes was analyzed at 37 or 30 °C. Interestingly, co-expression of *oas1b* and *abcf3* completely alleviated cell growth inhibition at both 37 °C (Fig. 6*C*) and 30 °C (Fig. 6*D*), suggesting that an intracellular interaction between ABCF3 and OAS1B had occurred.

The cellular distribution of each expressed protein was next analyzed. The cells induced at 30 or 37 °C were lysed, and the cytosolic, membrane, and IB fractions were prepared. The proteins in each fraction were separated by SDS-PAGE and detected by Western blotting with either anti-OAS1 or anti-ABCF3 antibody (Fig. 6, *E–H*). An 8–10-fold increase in the level of total (*T*) OAS1B in cells co-expressing *oas1b* and *abcf3*, compared with that in cells expressing *oas1b* alone, was observed both at 30 and 37 °C (Fig. 6, *G* and *H*, compare *lanes 5* and *9*, and *K* and *L*, *T*). However, the majority of the OAS1B protein produced under co-expression conditions was found in the IB fraction with about a 25-fold increase in the accumulation of OAS1B in IB at 37 °C compared with expression of OAS1B alone (Fig. 6, *G*, compare *lanes 2* and *6*, and *K*, *IB*). At 30 °C, a 20-fold higher level of OAS1B was observed in the IB fraction (Fig. 6, *H*, compare *lanes 2* and *6*; and *L*, *IB*) with lower OAS1B levels detected in the cytosolic and membrane fractions. The results indicate that due to the sequestration of overexpressed OAS1B in inclusion bodies at both temperatures, OAS1B localization to the membrane remained the same or decreased in co-expressing cells. Moreover, co-expression at 30 or 37 °C had little or no effect on the stability or cellular distribution of ABCF3 (Fig. 6, *I* and *J*).

Discussion

Recent studies have demonstrated the involvement of the full-length OAS1B protein in conferring a flavivirus resistance phenotype in mice (9, 61, 62). In yeast two-hybrid and subsequent *in vitro* pulldown experiments, ABCF3 and ORP1L were identified as potential OAS1B partners that may play a role in the flavivirus resistance mechanism (9). However, the specific roles of these partners in the resistance phenotype have not been determined.

In this study, a nonhydrolyzable analog TNP-ATP was used to gain an understanding of the nucleotide-binding properties of ABCF3. Interestingly, we found that TNP-ATP binding to ABCF3 follows allosteric kinetics and exhibits positive cooperativity with a Hill coefficient of 1.8. The two NBDs in ABCF3 are each thought to participate in forming an ATP-binding pocket (Fig. 5*E*), and the data obtained suggest cooperativity between the two pockets with binding of a nucleotide to one pocket in ABCF3 increasing the binding affinity of the other pocket. Conservative mutations (Lys to Arg) in the Walker A motif of either NBD resulted in a decrease in affinity for TNP-ATP, implying a role for each NBD in nucleotide binding. However, the NBD2 mutation (K531R) produced a much larger effect on TNP-ATP binding, suggesting an unequal contribution of the two NBDs. Results showing an unequal contribution of the two NBDs to the function of the bacterial ABCF protein Vga(A) were previously reported (38). Moreover, the NBD2 mutation in Vga(A) was found to be more detrimental than the NBD1 mutation, as seen in the case of ABCF3.

We determined that ABCF3 is an active ATPase with a basal ATPase activity of about 130 nmol/min/mg. Modulation of ABCF3 activity by several lipids and alkyl ether lipid-based amphiphilic drugs was observed, suggesting an ability of ABCF3 to directly bind these lipids and drugs. Although sphingosine, sphingomyelin, PAF, and LPC enhanced the activity, the alkyl ether lipids miltefosine, edelfosine, and perifosine, as well as LPI, lyso-PAF, and cholesterol either inhibited activity or produced a biphasic response. Alkyl ether lipids are derived from the glycerophospholipid LPC (63), and the results suggest that small changes in lipid structure can produce different effects on ABCF3 activity. Although it is currently not understood why some lipids enhance while others inhibit ABCF3 ATPase activity, differential effects of different substrates on the activities of other ABC proteins have been observed (45, 64, 65). Strong inhibition of the ATPase activity of Vga(A) and other ABCF proteins by their antibiotic substrates reported previously also suggested direct interaction with their substrates (22, 38).

Point mutations in the NBD1 and NBD2 of ABCF3 affected both basal and ligand-stimulated ATPase activity differently providing further evidence for the asymmetric nature of the two NBDs. Specifically, the NBD1 mutant K216A protein (containing intact pocket 2, Fig. 5*B*) exhibited significantly reduced basal activity, whereas the NBD2 mutant K531A protein (containing intact pocket 1, Fig. 5*C*) showed full basal activity. Furthermore, addition of sphingosine to proteins containing mutations in NBD1 resulted in a significantly higher stimulation of activity than observed with the WT protein (Fig. 5*B*), while the activity of proteins containing NBD2 mutations was not only unstimulated but was inhibited in response to sphingosine (Fig. 5*C*). Sphingosine also did not stimulate the ATPase activity of the K216A/K531A double mutant (Fig. 5*D*). Based on these observations, we assume that the 100% basal ATPase activity seen in K531A mutation results from the intact pocket P1 (Fig. 5*C*), and the high sphingosine stimulation seen in K216A comes from the intact pocket P2 (Fig. 5*B*). Therefore, we propose that pocket 1 is the site of basal catalysis, whereas pocket 2 engages in ligand-stimulated ATP hydrolysis (Fig. 5*E*). The inhibition of the ATPase activities of the NBD2 mutant proteins also suggests that sphingosine binding produces a dual effect, stimulating the ATPase activity of pocket 2 while inhibiting the activity of pocket 1 (Fig. 5, *C* and *E*).

The above data are consistent with the TNP-ATP binding analysis conducted in the presence of sphingosine. While sphingosine restored the binding affinity of the K216A mutant protein to WT levels, the binding occurred with a Hill coefficient of 1.1, suggesting that the enhanced TNP-ATP binding in the presence of sphingosine occurs predominantly to the intact pocket 2 (Fig. 5*B*). Interestingly, sphingosine-dependent TNP-ATP binding to WT ABCF3 also demonstrated a Hill coefficient of 1.0 in contrast to the cooperative binding seen in the absence of the ligand (Fig. 5*A*), indicating that in the presence of sphingosine only one site preferentially binds ATP, and this active site corresponds to pocket 2. Surprisingly, addition of

sphingosine to the pocket 2 mutant (K531A) or the double mutant (K216A/K531A) protein also resulted in overall high affinity TNP-ATP binding. In contrast to the K216A mutant protein, however, neither the pocket 2 mutant nor the double mutant showed any stimulation of ATPase activity by sphingosine (Fig. 5, *C* and *D*). Because TNP-ATP binding normally occurs with a much higher affinity than ATP binding (44, 55, 56), the simplest explanation for these data may be that sphingosine can enhance TNP-ATP binding to pocket 2 despite the presence of the K531A mutation, but it is unable to restore its catalytic function. Overall, these data indicate the importance of an intact pocket 2 in sphingosine-stimulated ATP binding and catalysis by ABCF3.

Both co-immunoprecipitation of OAS1B and ABCF3 from mammalian cells and co-localization of OAS1B and ABCF3 at the ER membrane of mammalian cells were previously shown (9). The OAS1B-tr protein, which does not contain a C-terminal transmembrane domain, is unable to localize to the ER and does not confer flavivirus resistance. Knockdown of ABCF3 in infected cells resulted in an increase in WNV yields but did not affect the yields of two nonflaviviruses, indicating that the action of ABCF3 is specific for flaviviruses. Furthermore, the effect of ABCF3 knockdown on WNV yields was observed in WNV-infected MEFs expressing full-length OAS1B but not in infected MEFs expressing OAS1B-tr, suggesting that interaction between ABCF3 and OAS1B at the ER plays a role in the OAS1B-mediated flavivirus resistance phenotype in infected cells (9). The data presented here provide strong, but indirect, evidence for interaction between OAS1B and ABCF3 in bacterial cells. We showed that the expression of OAS1B alone in *E. coli* results in varying degrees of growth inhibition, including complete growth arrest, depending on the copy number of the vector and the temperature of expression. This phenotype is consistent with the inhibitory effect produced by overexpression of some membrane proteins in bacterial cells (58, 66). Removal of the C-terminal domain of OAS1B containing the putative TM domain resulted in alleviation of growth inhibition, providing support for the proposal that OAS1B is a membrane-embedded protein (9). Furthermore, co-expression of full-length OAS1B with ABCF3 rescued the growth inhibitory phenotype produced by OAS1B expression alone at 30 °C or 37 °C, suggesting interaction between OAS1B and ABCF3. Co-expression also unexpectedly resulted in a striking increase in the cellular levels of OAS1B, indicating that ABCF3 protects OAS1B from degradation by cellular proteases. The majority of the OAS1B protein stabilized under the co-expression growth conditions at either 30 or 37 °C was, however, sequestered in an insoluble fraction in the cell. It is well-documented that the expression or overexpression of a heterologous membrane protein in bacteria can often result in toxic effects (67, 68), proteolysis by housekeeping proteases (69–72), and/or accumulation of the overexpressed protein in inclusion bodies (58, 59). Co-expression with an interacting partner protein has been previously shown to result in alleviation of toxicity and protection from proteolysis (69, 72, 73). We saw evidence of all these phenomena under different expression conditions: toxicity and proteolysis of OAS1B when it was expressed alone but alleviation of growth inhibition and stabilization of OAS1B, followed by sequestration in inclusion bodies, when co-expressed with ABCF3.

To our knowledge, interaction between eukaryotic proteins in bacterial cells has not been shown previously. The pETDuet-1–based bacterial co-expression system described here is not only ideal for examining protein complexes (74–76), but it also offers several distinct advantages for advancing knowledge of the two proteins. The availability of a clear growth phenotype (growth inhibition/rescue) could be used to develop a genetic screen for further analyzing the domains involved in interaction between OAS1B and ABCF3. For example, the linker domain of ABCF3 may play a role in interaction with OAS1B. The effect of mutations and/or deletions in this and other domains of either ABCF3 or OAS1B could be tested in the bacterial system by a simple growth inhibition/rescue assay. Furthermore, stabilization of large amounts of OAS1B by ABCF3 and the resulting sequestration in inclusion bodies was unexpected, and this could be utilized to prepare large amounts of OAS1B for biochemical and structural analysis in the future. Some eukaryotic proteins have previously been genetically manipulated to promote inclusion body formation and then recovered from inclusion bodies by solubilization and refolding into a functional form (77, 78). Functional integration of OAS1B and ABCF3 into bacterial membranes may also be achievable in the future through further optimization of low-level expression (66, 79, 80), as was previously shown for G protein–coupled receptors (81–83).

In conclusion, we showed that the mouse ABCF3 is an active ATPase, and its activity is modulated by several lipids, including sphingosine and sphingomyelin, two lipids previously shown to have altered levels in flavivirus-infected cells (50–52). High levels of ATP have been shown to be required for efficient viral RNA synthesis inside membrane replication vesicles (84, 85). The dengue NS3 helicase unwinds dsRNA templates in the presence of high levels of ATP but anneals complementary RNA strands when ATP levels are low (86). Although OAS1B protein is not an active 2–5A synthetase, we found it to have an ATPase activity of about 90 nmol/min/mg (Fig. S4, *A–C*). Therefore, the ABCF3–OAS1B complex, which is anchored in the endoplasmic reticular membrane, may contribute to the reduced level of viral RNA production characteristic of the flavivirus resistance phenotype through its ATP binding and hydrolysis activities, which may be modulated by lipids as shown in this study.

Experimental procedures

Reagents and antibodies

All reagents were purchased from Sigma unless otherwise noted. 2′(3′)-*O*-(2,4,6-trinitrophenyl)adenosine 5′-triphosphate was purchased from Molecular Probes, Inc., and stored at −20 °C in the dark; Hoechst 33342 was from Invitrogen; edelfosine, cholesterol, 10:0 phosphatidylcholine (10:0 PC), 14:0 phosphatidylethanolamine (14:0 PE), LPC, LPI, sphingosine, sphingosine 1-phosphate, sphingomyelin, PAF, lyso-PAF, ceramide, and dihydroceramide were from Avanti Polar Lipids, Inc.; Glutathione Sepharose 4B and PreScission Protease were from GE Healthcare; and HisPur™ Ni-NTA resin was pur-

chased from Thermo Fisher Scientific. Nucleotides, pH 7.5, and drugs were prepared in distilled deionized water unless otherwise stated. Cholesterol, sphingosine, sphingosine 1-phosphate, PAF, lyso-PAF, LPC, LPI, alkyl ether lipids, ceramide, dihydroceramide, and quinidine were prepared in ethanol prior to use. 10:0 PC and 14:0 PE were prepared in a buffer consisting of 50 mM MOPS, 125 mM NaCl, pH 7.5, and sonicated before use.

Subcloning of abcf3 and oas1b

A TOPO® XL PCR cloning kit (Invitrogen) was used to clone *abcf3* or *oas1b* into the pCR®-XL-TOPO® vector (pCR). The *abcf3* gene was subcloned from pCR-*abcf3* into pUC18 using EcoRI and XbaI, into pET-Duet-1 (pED) using NdeI and AvrII, and into pGEX-6p-1 (pGEX) using EcoRI and XhoI restriction sites. *abcf3* was then subcloned from pGEX-*abcf3* into pET28a using EcoRI and XhoI restriction sites. The pGEX-*abcf3* and pET28a-*abcf3* clones express ABCF3 containing an N-terminal GST-tag and His-tag, respectively.

The *oas1b* gene was subcloned from pCR-*oas1b* into pSU2718 using PstI and HindIII, into pED using NcoI and BamHI, and into the pGEX-6p-1 vector using BamHI and EcoRI restriction sites. A C-terminally truncated version of *oas1b,* named *oas1b*(Δ*tm*), was amplified using a forward primer containing a BamHI restriction site and a reverse primer containing a stop codon after nucleotide 1059 of *oas1b* followed by an EcoRI restriction site. The *oas1b*(Δ*tm*) fragment was then subcloned into the pGEX-6p-1 vector using BamHI and EcoRI restriction sites to generate pCR-*oas1b*(Δ*tm*). To create the double-expression clone pED-*oas1b-abcf3*, *oas1b* from pCR-*oas1b* was subcloned into pED-*abcf3* using NcoI and BamHI restriction sites. The pED clones (referred to as pED*1b*, pED*f3*, and pED*1bf3*) express ABCF3 and/or OAS1B protein without a tag.

Media, growth, isolation, and analysis of cell fractions

E. coli Rosetta 2(DE3)pLysS cells containing pED, pED*1b*, pED*f3*, or pED*1bf3* were grown in 50 ml of LB medium with ampicillin (100 μg/ml) at 37 °C overnight. The next day these cultures were diluted 1:50 into 250 ml of fresh LB with ampicillin in a 1-liter flask and incubated at 37 °C until the mid-log phase was reached ($A_{600\,nm}$ = 0.6). The cultures were then induced with 0.25 mM IPTG and incubated at 37 or 30 °C for 3 h following induction. Cells in 100 ml of culture media obtained under different growth conditions were pelleted by centrifugation. The pellets were resuspended in 3 ml of 1× PBS buffer, pH 7.4, containing 20% glycerol (Buffer A), 1 mM DTT, and protease cocktail inhibitor (Roche Diagnostics). Samples were lysed twice by passage through a mini-French pressure cell (Thermo Electron Corp.) at 16,000 p.s.i. to obtain a total cell lysate. After centrifugation at 13,000 × *g* for 20 min at 4 °C, the inclusion body (pellet) was collected, and the supernatant was centrifuged at 100,000 × *g* for 1 h to obtain the cytosol (supernatant) and the membrane (pellet). The membrane and the inclusion body pellets were resuspended in 250 and 500 μl, respectively, of Buffer A containing 1 mM DTT. The protein concentration of each fraction was determined with a DC™ assay (Bio-Rad).

Western blot analysis

ABCF3 or OAS1B in cellular fractions and as purified proteins were detected by Western blotting. Proteins were separated by 10% SDS-PAGE, and then transferred to a nitrocellulose membrane for 16 h at 4 °C. An equal amount of protein was loaded per well unless otherwise indicated in the figure legends. After transfer, the membranes were blocked with 0.2% nonfat dry milk for ABCF3 and 5% BSA for OAS1B. Membranes were incubated with either anti-OAS1 antibody at 4 °C for at least 16 h or with anti-ABCF3 antibody for 1 h at room temperature. Rabbit anti-ABCF3 polyclonal antibody (Bethyl Laboratories, Inc.) was diluted 1:2000 with 0.2% nonfat dry milk in 1× TTBS (1% Tween 20 in 20 mM Tris, 500 mM NaCl, pH 7.5). Rabbit anti-OAS1 polyclonal antibody (Abcam Inc.) was diluted to 1:500 with 1% BSA in 1× TTBS. Secondary anti-rabbit goat IgG antibodies obtained from Bio-Rad were diluted to 1:3000 in 0.2% nonfat dry milk in 1× TTBS for ABCF3 or 1% BSA in 1× TTBS for OAS1B detection.

Densitometric scanning and quantification

The nitrocellulose membranes were scanned, and Multi-Gauge version 2.3 software was used for quantification of protein band intensity. The expression of ABCF3 or OAS1B under single expression conditions was designated as 1.0. A fold-change in expression of each protein under double expression conditions was calculated by dividing the amount of each protein in a double expression sample by the amount in a single expression sample from the same gel. Data from at least three independent experiments were combined to obtain average relative expression values.

Purification of GST-tagged ABCF3

E. coli Rosetta 2(DE3)pLysS cells containing pGEX plasmids were grown in 1 liter of LB medium with ampicillin (100 μg/ml) at 37 °C until mid-log phase was reached ($A_{600\,nm}$ = 0.6) and then induced with 0.25 mM IPTG at 20 °C for 16 h. ABCF3 protein was purified after expression from the pGEX*f3* clone according to the manufacturer's instructions (GE Healthcare) with some modifications. The cell pellets were resuspended in 50 ml of Buffer A containing 10 mM DTT and complete protease inhibitor cocktail. The cells were broken by two passages through a French press followed by centrifugation as described above. The supernatant was mixed with 1.3 ml of washed Glutathione Sepharose (GE Healthcare) for 16 h in a tube revolver at 10 rpm and then transferred to a 10-ml gravity-flow column. To obtain uncleaved GST–ABCF3 protein, the column was washed with three 10-column volumes of Buffer A with 1 mM DTT and eluted twice with 1 ml of 10 mM glutathione in 50 mM Tris-HCl, pH 8.0, with 20% glycerol. To obtain ABCF3 without the GST tag, the column was washed five times with 10 column volumes, three times with Buffer A, and two times with 1× cleavage buffer (GE Healthcare) containing 20% glycerol and 1 mM DTT (Buffer B). The washed sepharose was then removed from the column, mixed with 920 μl of Buffer B and 80 μl of PreScission protease in an Eppendorf tube, and incubated on a tube revolver for 4 h (10 rpm) at 4 °C. The sepharose was then added back to the column, and the cleaved ABCF3 was eluted from the column twice with 1 ml of Buffer B. The protein con-

centration was determined using the DC™ assay (Bio-Rad), and aliquots were stored at −80 °C until use.

Purification of His-tagged ABCF3

E. coli HMS174(DE3) cells transformed with pET28a DNA encoding the WT or a mutant *abcf3* gene were grown in 1 liter of LB medium with kanamycin (30 μg/ml) at 37 °C until mid-log phase was reached ($A_{600\ nm}$ = 0.6) and induced with 0.25 mM IPTG at 20 °C for 16 h. The cells were pelleted, the cell pellet was resuspended in 10 ml of Buffer A containing 1 mM DTT and complete protease inhibitor, and the cells were lysed with a French press followed by centrifugation as described above. The supernatant was then mixed with 2 ml of Ni-NTA–agarose (previously washed with 40 ml of Buffer A containing 10 mM imidazole) in a closed 10-ml gravity-flow column on a tube revolver at 10 rpm for 1 h at 4 °C. The flow-through was collected, and the column was washed with 50 ml of 30 mM imidazole and 1 ml of 100 mM imidazole. The ABCF3 protein was then eluted twice with 1 ml of Buffer A containing 200 mM imidazole. The two elutions were separately dialyzed against 500 ml of Buffer A overnight and again for 2 h the next day before collection. Protein concentration was determined by the DC™ assay (Bio-Rad), and aliquots were stored at −80 °C until use.

Site-directed mutagenesis of the Walker A or Walker B motifs of ABCF3

Site-directed mutagenesis of the *abcf3* gene was performed using a QuickChange site-directed mutagenesis kit (Stratagene, La Jolla, CA). Mutations in the Walker A (K216A, K531A, K216R, and K531R) or Walker B (E353A, E636A, E353Q, and E636Q) domain of each NBD were created using the pET28a-*abcf3* plasmid as a template. Plasmid DNA with a single mutation in one NBD was used as the template to make a second mutation in the other NBD creating the double Walker A (K216A/K531A and K216R/K531R) or the double Walker B (E353A/E636A and E353Q/E636Q) mutants.

ATPase activity assay

The ATPase activity of 5 μg of purified WT or mutant ABCF3 protein was determined using an ATPase activity assay, as described previously (44, 87). The slope of the reaction was measured between 200 and 400 s and used to determine the ATPase activity in nanomoles/min/mg. Different concentrations of a ligand were added to 5 μg of purified ABCF3 in a 1-ml reaction volume.

Analysis of TNP-ATP binding to ABCF3

TNP-ATP binding assays were conducted with purified WT or mutant ABCF3 proteins. TNP-ATP (0.1 to 20 μM) was added sequentially to 5 μM ABCF3 in Buffer A in a total starting volume of 500 μl in each titration. The titrations were performed on an Alphascan-2 spectrofluorometer (Photon Technology International, London, Ontario, Canada) with the following settings: 1.00-mm slit widths at 75 watts with 403 nm excitation and 450–600 nm emission. To determine the increase in fluorescence resulting from TNP-ATP binding to the protein, values obtained from a negative control titration without any added ABCF3 were subtracted from the respective fluorescence values obtained in reactions containing ABCF3. The fluorescence units obtained were then corrected for inner filter effects using Equation 1 (88),

$$F_{i,\,cor} = (F_i - F_B)(V_i/V_0) \times 10^{0.5b(A_{\lambda ex} + A_{\lambda em})} \quad \text{(Eq. 1)}$$

In Equation 1, $F_{i,\,cor}$ is the revised fluorescence intensity value based on inner filter effects; F_i corresponds to the preliminary fluorescence values; F_B is the fluorescence for the blank (no protein) titration at a given point; V_0 is the starting sample volume; V_i is the sample volume at a given point in the titration; b is the optical cell path length measured in centimeters; and $A_{\lambda ex}$ is the absorbance at 403 nm excitation with $A_{\lambda em}$ the absorbance at emission wavelength 548 nm.

Percent increase in fluorescence was then obtained by using Equation 2,

$$\%\ \text{increase} = ((F_{i,\,cor} - F_{0,\,cor})/(F_{f,\,cor})) \times 100 \quad \text{(Eq. 2)}$$

In Equation 2, $F_{i,\,cor}$ is the fluorescence intensity value corrected at a given point in the titration, $F_{0,\,cor}$ is the initial corrected fluorescence value for the initial titration value, and $F_{f,\,cor}$ is the final corrected fluorescence value for the titration. Nonlinear regression in GraphPad Prism 6 Software was used to analyze binding kinetics based on a single site, two site, or allosteric model for binding.

TNP-ATP displacement assays

To determine whether TNP-ATP binds to the nucleotide-binding pocket(s) of ABCF3, titrations were performed with increasing concentrations of ATP (0.1–20 mM), ADP (0.1–20 mM), or AMP (0.1–20 mM). Briefly, 5 μM ABCF3 was mixed with 5 μM TNP-ATP and 10 mM $MgCl_2$ in 500 μl of Buffer A, and the reaction was incubated at room temperature for 5 min before starting the assay (55, 56). Increasing amounts of nucleotide were then added to the sample, and the fluorescence was monitored. For each experiment, a blank titration (sample prepared without ABCF3) was also performed. The fluorescence values were corrected for inner filter effects according to Equation 1 above.

Intrinsic Trp fluorescence quenching analysis

Intrinsic Trp fluorescence of ABCF3 was determined on an Alphascan-2 spectrofluorometer (Photon Technology International, London, Ontario, Canada) with the following settings: 1.00-mm slit widths at 75 watts with 295 nm excitation and 310–370 nm emission. Quenching of intrinsic fluorescence by ATP or ADP was then determined by titrating increasing amounts of nucleotide (5 μM to 5 mM) into a 500 μl reaction volume containing Buffer A and 0.5 μM purified ABCF3 protein. Control titrations containing 10 μM NATA in the 500 μl reaction volume described above were also carried out with ATP or ADP to determine the degree of nonspecific quenching of tryptophan fluorescence. All fluorescence values obtained were corrected for inner filter effects with Equation 1, using 295 nm excitation for $A_{\lambda ex}$ and 330 nm emission for $A_{\lambda em}$. Percent quenching was then obtained with Equation 3,

$$\%\ \text{quenching} = ((F_{0,\,cor} - F_{i,\,cor})/(F_{0,\,cor})) \times 100 \quad \text{(Eq. 3)}$$

In Equation 3, $F_{i,\,cor}$ and $F_{0,\,cor}$ are the same values as described above. Kinetic analysis was performed using nonlinear regression with GraphPad Prism 6 software using one- or two-site binding kinetics.

Author contributions—E. P., M. A. B., and P. K. conceptualization; E. P., M. A. B., and P. K. formal analysis; E. P. and P. K. supervision; E. P., M. A. B., and P. K. funding acquisition; E. P., E. S., and P. K. investigation; E. P., E. S., and P. K. methodology; E. P., M. A. B., and P. K. writing-original draft; E. P. and P. K. project administration.

Acknowledgments—We thank Chao Zhao for making the pGEX- and pED-based clones used in these experiments and the Biotech Core Facilities at Georgia State University for use of instrumentation.

References

1. Brinton, M. A. (1996) in *Viral Pathogenesis* (Ahmed, R., and Nathanson, N., eds) pp. 303–328, Lippincott-Raven Publishers, Philadelphia
2. Mashimo, T., Lucas, M., Simon-Chazottes, D., Frenkiel, M. P., Montagutelli, X., Ceccaldi, P. E., Deubel, V., Guenet, J. L., and Despres, P. (2002) A nonsense mutation in the gene encoding 2′–5′-oligoadenylate synthetase/L1 isoform is associated with West Nile virus susceptibility in laboratory mice. *Proc. Natl. Acad. Sci. U.S.A.* **99,** 11311–11316 CrossRef Medline
3. Perelygin, A. A., Scherbik, S. V., Zhulin, I. B., Stockman, B. M., Li, Y., and Brinton, M. A. (2002) Positional cloning of the murine flavivirus resistance gene. *Proc. Natl. Acad. Sci. U.S.A.* **99,** 9322–9327 CrossRef Medline
4. Silverman, R. H. (2007) Viral encounters with 2′,5′-oligoadenylate synthetase and RNase L during the interferon antiviral response. *J. Virol.* **81,** 12720–12729 CrossRef Medline
5. Kakuta, S., Shibata, S., and Iwakura, Y. (2002) Genomic structure of the mouse 2′,5′-oligoadenylate synthetase gene family. *J. Interferon Cytokine Res.* **22,** 981–993 CrossRef Medline
6. Perelygin, A. A., Zharkikh, A. A., Scherbik, S. V., and Brinton, M. A. (2006) The mammalian 2′–5′-oligoadenylate synthetase gene family: evidence for concerted evolution of paralogous Oas1 genes in *Rodentia* and *Artiodactyla*. *J. Mol. Evol.* **63,** 562–576 CrossRef Medline
7. Elkhateeb, E., Tag-El-Din-Hassan, H. T., Sasaki, N., Torigoe, D., Morimatsu, M., and Agui, T. (2016) The role of mouse 2′,5′-oligoadenylate synthetase 1 paralogs. *Infect. Genet. Evol.* **45,** 393–401 CrossRef Medline
8. Elbahesh, H., Jha, B. K., Silverman, R. H., Scherbik, S. V., and Brinton, M. A. (2011) The Flvr-encoded murine oligoadenylate synthetase 1b (Oas1b) suppresses 2–5A synthesis in intact cells. *Virology* **409,** 262–270 CrossRef Medline
9. Courtney, S. C., Di, H., Stockman, B. M., Liu, H., Scherbik, S. V., and Brinton, M. A. (2012) Identification of novel host cell binding partners of Oas1b, the protein conferring resistance to flavivirus-induced disease in mice. *J. Virol.* **86,** 7953–7963 CrossRef Medline
10. Paul, D., and Bartenschlager, R. (2015) Flaviviridae replication organelles: oh, what a tangled web we weave. *Annu. Rev. Virol.* **2,** 289–310 CrossRef Medline
11. Vihervaara, T., Uronen, R. L., Wohlfahrt, G., Björkhem, I., Ikonen, E., and Olkkonen, V. M. (2011) Sterol binding by OSBP-related protein 1L regulates late endosome motility and function. *Cell. Mol. Life Sci.* **68,** 537–551 CrossRef Medline
12. ter Beek, J., Guskov, A., and Slotboom, D. J. (2014) Structural diversity of ABC transporters. *J. Gen. Physiol.* **143,** 419–435 CrossRef Medline
13. Qu, L., Jiang, Y., Cheng, C., Wu, D., Meng, B., Chen, Z., Zhu, Y., Shaw, N., Ouyang, S., and Liu, Z. J. (2018) Crystal structure of ATP-bound human ABCF1 demonstrates a unique conformation of ABC proteins. *Structure* **26,** 1259–1265.e3 CrossRef Medline
14. Davidson, A. L., Dassa, E., Orelle, C., and Chen, J. (2008) Structure, function, and evolution of bacterial ATP-binding cassette systems. *Microbiol. Mol. Biol. Rev.* **72,** 317–364 CrossRef Medline
15. Holland, I. B. (2003) *ABC Proteins: From Bacteria to Man*, 1st. Ed., pp. 14–16, Academic Press, San Diego
16. Ambrose, K. D., Nisbet, R., and Stephens, D. S. (2005) Macrolide efflux in *Streptococcus pneumoniae* is mediated by a dual efflux pump (mel and mef) and is erythromycin inducible. *Antimicrob. Agents Chemother.* **49,** 4203–4209 CrossRef Medline
17. Nunez-Samudio, V., and Chesneau, O. (2013) Functional interplay between the ATP binding cassette Msr(D) protein and the membrane facilitator superfamily Mef(E) transporter for macrolide resistance in *Escherichia coli*. *Res. Microbiol.* **164,** 226–235 CrossRef Medline
18. Sharkey, L. K., Edwards, T. A., and O'Neill, A. J. (2016) ABC-F proteins mediate antibiotic resistance through ribosomal protection. *MBio* **7,** e01975 CrossRef Medline
19. Wilson, D. N. (2016) The ABC of ribosome-related antibiotic resistance. *MBio* **7,** e00598-16 10.1128/mBio.00598-16 Medline
20. Lenart, J., Vimberg, V., Vesela, L., Janata, J., and Balikova Novotna, G. (2015) Detailed mutational analysis of Vga(A) interdomain linker: implication for antibiotic resistance specificity and mechanism. *Antimicrob. Agents Chemother.* **59,** 1360–1364 CrossRef Medline
21. Murina, V., Kasari, M., Hauryliuk, V., and Atkinson, G. C. (2018) Antibiotic resistance ABCF proteins reset the peptidyl transferase centre of the ribosome to counter translational arrest. *Nucleic Acids Res.* **46,** 3753–3763 CrossRef Medline
22. Daniel, J., Abraham, L., Martin, A., Pablo, X., and Reyes, S. (2018) Rv2477c is an antibiotic-sensitive manganese-dependent ABC-F ATPase in *Mycobacterium tuberculosis*. *Biochem. Biophys. Res. Commun.* **495,** 35–40 CrossRef Medline
23. Boël, G., Smith, P. C., Ning, W., Englander, M. T., Chen, B., Hashem, Y., Testa, A. J., Fischer, J. J., Wieden, H. J., Frank, J., Gonzalez, R. L., Jr., and Hunt, J. F. (2014) The ABC-F protein EttA gates ribosome entry into the translation elongation cycle. *Nat. Struct. Mol. Biol.* **21,** 143–151 CrossRef Medline
24. Chen, B., Boël, G., Hashem, Y., Ning, W., Fei, J., Wang, C., Gonzalez, R. L., Jr., Hunt, J. F., and Frank, J. (2014) EttA regulates translation by binding the ribosomal E site and restricting ribosome-tRNA dynamics. *Nat. Struct. Mol. Biol.* **21,** 152–159 CrossRef Medline
25. Paytubi, S., Morrice, N. A., Boudeau, J., and Proud, C. G. (2008) The N-terminal region of ABC50 interacts with eukaryotic initiation factor eIF2 and is a target for regulatory phosphorylation by CK2. *Biochem. J.* **409,** 223–231 CrossRef Medline
26. Dong, J., Lai, R., Jennings, J. L., Link, A. J., and Hinnebusch, A. G. (2005) The novel ATP-binding cassette protein ARB1 is a shuttling factor that stimulates 40S and 60S ribosome biogenesis. *Mol. Cell. Biol.* **25,** 9859–9873 CrossRef Medline
27. Marton, M. J., Vazquez de Aldana, C. R., Qiu, H., Chakraburtty, K., and Hinnebusch, A. G. (1997) Evidence that GCN1 and GCN20, translational regulators of GCN4, function on elongating ribosomes in activation of eIF2α kinase GCN2. *Mol. Cell. Biol.* **17,** 4474–4489 CrossRef Medline
28. Vazquez de Aldana, C. R., Marton, M. J., and Hinnebusch, A. G. (1995) GCN20, a novel ATP binding cassette protein, and GCN1 reside in a complex that mediates activation of the eIF-2α kinase GCN2 in amino acid-starved cells. *EMBO J.* **14,** 3184–3199 CrossRef Medline
29. Tyzack, J. K., Wang, X., Belsham, G. J., and Proud, C. G. (2000) ABC50 interacts with eukaryotic initiation factor 2 and associates with the ribosome in an ATP-dependent manner. *J. Biol. Chem.* **275,** 34131–34139 CrossRef Medline
30. Skogerson, L., and Wakatama, E. (1976) A ribosome-dependent GTPase from yeast distinct from elongation factor 2. *Proc. Natl. Acad. Sci. U.S.A.* **73,** 73–76 CrossRef Medline
31. Andersen, C. B., Becker, T., Blau, M., Anand, M., Halic, M., Balar, B., Mielke, T., Boesen, T., Pedersen, J. S., Spahn, C. M., Kinzy, T. G., Andersen, G. R., and Beckmann, R. (2006) Structure of eEF3 and the mechanism of transfer RNA release from the E-site. *Nature* **443,** 663–668 CrossRef Medline
32. Kurata, S., Nielsen, K. H., Mitchell, S. F., Lorsch, J. R., Kaji, A., and Kaji, H. (2010) Ribosome recycling step in yeast cytoplasmic protein synthesis is catalyzed by eEF3 and ATP. *Proc. Natl. Acad. Sci. U.S.A.* **107,** 10854–10859 CrossRef Medline

33. Triana-Alonso, F. J., Chakraburtty, K., and Nierhaus, K. H. (1995) The elongation factor 3 unique in higher fungi and essential for protein biosynthesis is an E site factor. *J. Biol. Chem.* **270,** 20473–20478 CrossRef Medline
34. Lee, M. N., Roy, M., Ong, S. E., Mertins, P., Villani, A. C., Li, W., Dotiwala, F., Sen, J., Doench, J. G., Orzalli, M. H., Kramnik, I., Knipe, D. M., Lieberman, J., Carr, S. A., and Hacohen, N. (2013) Identification of regulators of the innate immune response to cytosolic DNA and retroviral infection by an integrative approach. *Nat. Immunol.* **14,** 179–185 CrossRef Medline
35. Guo, F., Ding, Y., Caberoy, N., Alvarado, G., Wang, F., Chen, R., and Li, W. (2015) ABCF1 extrinsically regulates retinal pigment epithelial cell phagocytosis. *Mol. Biol. Cell* **26,** 2311–2320 CrossRef Medline
36. Ando-Akatsuka, Y., Shimizu, T., Numata, T., and Okada, Y. (2012) Involvements of the ABC protein ABCF2 and α-actinin-4 in regulation of cell volume and anion channels in human epithelial cells. *J. Cell. Physiol.* **227,** 3498–3510 CrossRef Medline
37. Zhou, J., Lin, Y., Shi, H., Huo, K., and Li, Y. (2013) hABCF3, a TPD52L2 interacting partner, enhances the proliferation of human liver cancer cell lines *in vitro*. *Mol. Biol. Rep.* **40,** 5759–5767 CrossRef Medline
38. Jacquet, E., Girard, J. M., Ramaen, O., Pamlard, O., Lévaique, H., Betton, J. M., Dassa, E., and Chesneau, O. (2008) ATP hydrolysis and pristinamycin IIA inhibition of the *Staphylococcus aureus* Vga(A), a dual ABC protein involved in streptogramin A resistance. *J. Biol. Chem.* **283,** 25332–25339 CrossRef Medline
39. Murat, D., Bance, P., Callebaut, I., and Dassa, E. (2006) ATP hydrolysis is essential for the function of the Uup ATP-binding cassette ATPase in precise excision of transposons. *J. Biol. Chem.* **281,** 6850–6859 CrossRef Medline
40. Murina, V., Kasari, M., Takada, H., Hinnu, M., Saha, C. K., Grimshaw, J. W., Seki, T., Reith, M., Putrins, M., Tenson, T., Strahl, H., Hauryliuk, V., and Atkinson, G. C. (2018) ABCF ATPases involved in protein synthesis, ribosome assembly and antibiotic resistance: structural and functional diversification across the Tree of Life. *J. Mol. Biol.* 2018, S0022-2836(18)31288-9 CrossRef Medline
41. Putman, M., Koole, L. A., van Veen, H. W., and Konings, W. N. (1999) The secondary multidrug transporter LmrP contains multiple drug interaction sites. *Biochemistry* **38,** 13900–13905 CrossRef Medline
42. Liu, R., Siemiarczuk, A., and Sharom, F. J. (2000) Intrinsic fluorescence of the P-glycoprotein multidrug transporter: sensitivity of tryptophan residues to binding of drugs and nucleotides. *Biochemistry* **39,** 14927–14938 CrossRef Medline
43. Li, W., Sharma, M., and Kaur, P. (2014) The DrrAB efflux system of *Streptomyces peucetius* is a multidrug transporter of broad substrate specificity. *J. Biol. Chem.* **289,** 12633–12646 CrossRef Medline
44. Rahman, S. J., and Kaur, P. (2018) Conformational changes in a multidrug resistance ABC transporter DrrAB: fluorescence-based approaches to study substrate binding. *Arch. Biochem. Biophys.* **658,** 31–45 CrossRef Medline
45. Eckford, P. D., and Sharom, F. J. (2008) Functional characterization of *Escherichia coli* MsbA: interaction with nucleotides and substrates. *J. Biol. Chem.* **283,** 12840–12850 CrossRef Medline
46. Telbisz Á., Hegedüs, C., Váradi, A., Sarkadi, B., and Özvegy-Laczka, C. (2014) Regulation of the function of the human ABCG2 multidrug transporter by cholesterol and bile acids: effects of mutations in potential substrate and steroid binding sites. *Drug Metab. Dispos.* **42,** 575–585 CrossRef Medline
47. Clay, A. T., Lu, P., and Sharom, F. J. (2015) Interaction of the P-glycoprotein multidrug transporter with sterols. *Biochemistry* **54,** 6586–6597 CrossRef Medline
48. Eckford, P. D., and Sharom, F. J. (2006) P-glycoprotein (ABCB1) interacts directly with lipid-based anti-cancer drugs and platelet-activating factors. *Biochem. Cell Biol.* **84,** 1022–1033 CrossRef Medline
49. Quazi, F., and Molday, R. S. (2013) Differential phospholipid substrates and directional transport by ATP-binding cassette proteins ABCA1, ABCA7, and ABCA4 and disease-causing mutants. *J. Biol. Chem.* **288,** 34414–34426 CrossRef Medline
50. Martín-Acebes, M. A., Vázquez-Calvo, Á., and Saiz, J. C. (2016) Lipids and flaviviruses, present and future perspectives for the control of dengue, Zika, and West Nile viruses. *Prog. Lipid Res.* **64,** 123–137 CrossRef Medline
51. Perera, R., Riley, C., Isaac, G., Hopf-Jannasch, A. S., Moore, R. J., Weitz, K. W., Pasa-Tolic, L., Metz, T. O., Adamec, J., and Kuhn, R. J. (2012) Dengue virus infection perturbs lipid homeostasis in infected mosquito cells. *PLoS Pathog.* **8,** e1002584 CrossRef Medline
52. Chotiwan, N., Andre, B. G., Sanchez-Vargas, I., Islam, M. N., Grabowski, J. M., Hopf-Jannasch, A., Gough, E., Nakayasu, E., Blair, C. D., Belisle, J. T., Hill, C. A., Kuhn, R. J., and Perera, R. (2018) Dynamic remodeling of lipids coincides with dengue virus replication in the midgut of *Aedes aegypti* mosquitoes. *PLoS Pathog.* **14,** e1006853 CrossRef Medline
53. Osuna-Ramos, J. F., Reyes-Ruiz, J. M., and Del Ángel, R. M. (2018) The role of host cholesterol during flavivirus infection. *Front. Cell. Infect. Microbiol.* **8,** 388 CrossRef Medline
54. Jacquemyn, J., Cascalho, A., and Goodchild, R. E. (2017) The ins and outs of endoplasmic reticulum-controlled lipid biosynthesis. *EMBO Rep.* **18,** 1905–1921 CrossRef Medline
55. Stewart, R. C., VanBruggen, R., Ellefson, D. D., and Wolfe, A. J. (1998) TNP-ATP and TNP-ADP as probes of the nucleotide binding site of CheA, the histidine protein kinase in the chemotaxis signal transduction pathway of *Escherichia coli*. *Biochemistry* **37,** 12269–12279 CrossRef Medline
56. Plesniak, L., Horiuchi, Y., Sem, D., Meinenger, D., Stiles, L., Shaffer, J., Jennings, P. A., and Adams, J. A. (2002) Probing the nucleotide binding domain of the osmoregulator EnvZ using fluorescent nucleotide derivatives. *Biochemistry* **41,** 13876–13882 CrossRef Medline
57. Yao, H., and Hersh, L. B. (2006) Characterization of the binding of the fluorescent ATP analog TNP-ATP to insulysin. *Arch. Biochem. Biophys.* **451,** 175–181 CrossRef Medline
58. Wagner, S., Baars, L., Ytterberg, A. J., Klussmeier, A., Wagner, C. S., Nord, O., Nygren, P.-A., van Wijk, K. J., and de Gier, J.-W. (2007) Consequences of membrane protein overexpression in *Escherichia coli*. *Mol. Cell. Proteomics* **6,** 1527–1550 CrossRef Medline
59. Villaverde, A., Corchero, J. L., Seras-Franzoso, J., and Garcia-Fruitós, E. (2015) Functional protein aggregates: just the tip of the iceberg. *Nanomedicine* **10,** 2881–2891 CrossRef Medline
60. Martinez, E., Bartolomé, B., and de la Cruz, F. (1988) pACYC184-derived cloning vectors containing the multiple cloning site and lacZ alpha reporter gene of pUC8/9 and pUC18/19 plasmids. *Gene* **68,** 159–162 CrossRef Medline
61. Scherbik, S. V., Kluetzman, K., Perelygin, A. A., and Brinton, M. A. (2007) Knock-in of the Oas1b (r) allele into a flavivirus-induced disease susceptible mouse generates the resistant phenotype. *Virology* **368,** 232–237 CrossRef Medline
62. Kajaste-Rudnitski, A., Mashimo, T., Frenkiel, M. P., Guénet, J. L., Lucas, M., and Desprès, P. (2006) The 2′,5′-oligoadenylate synthetase 1b is a potent inhibitor of West Nile virus replication inside infected cells. *J. Biol. Chem.* **281,** 4624–4637 CrossRef Medline
63. Jaffrès, P. A., Gajate, C., Bouchet, A. M., Couthon-Gourvès, H., Chantôme, A., Potier-Cartereau, M., Besson, P., Bougnoux, P., Mollinedo, F., and Vandier, C. (2016) Alkyl ether lipids, ion channels and lipid raft reorganization in cancer therapy. *Pharmacol. Ther.* **165,** 114–131 CrossRef Medline
64. Urbatsch, I. L., and Senior, A. E. (1995) Effects of lipids on ATPase activity of purified Chinese hamster P-glycoprotein. *Arch. Biochem. Biophys.* **316,** 135–140 CrossRef Medline
65. Ambudkar, S. V., Lelong, I. H., Zhang, J., Cardarelli, C. O., Gottesman, M. M., and Pastan, I. (1992) Partial purification and reconstitution of the human multidrug-resistance pump: characterization of the drug-stimulatable ATP hydrolysis. *Proc. Natl. Acad. Sci. U.S.A.* **89,** 8472–8476 CrossRef Medline
66. Laage, R., and Langosch, D. (2001) Strategies for prokaryotic expression of eukaryotic membrane proteins. *Traffic* **2,** 99–104 CrossRef Medline
67. Wagner, S., Bader, M. L., Drew, D., and de Gier, J.-W. (2006) Rationalizing membrane protein overexpression. *Trends Biotechnol.* **24,** 364–371 CrossRef Medline
68. Gubellini, F., Verdon, G., Karpowich, N. K., Luff, J. D., Boël, G., Gauthier, N., Handelman, S. K., Ades, S. E., and Hunt, J. F. (2011) Physiological

response to membrane protein overexpression in *E. coli*. *Mol. Cell. Proteomics* **10,** M111.007930 CrossRef Medline
69. Li, W., Rao, D. K., and Kaur, P. (2013) Dual role of the metalloprotease FtsH in biogenesis of the DrrAB drug transporter. *J. Biol. Chem.* **288,** 11854–11864 CrossRef Medline
70. Ito, K., and Akiyama, Y. (2005) Cellular functions, mechanism of action, and regulation of FtsH protease. *Annu. Rev. Microbiol.* **59,** 211–231 CrossRef Medline
71. Akiyama, Y. (2009) Quality control of cytoplasmic membrane proteins in *Escherichia coli*. *J. Biochem.* **146,** 449–454 CrossRef Medline
72. Akiyama, Y., Kihara, A., Tokuda, H., and Ito, K. (1996) FtsH (HflB) is an ATP-dependent protease selectively acting on SecY and some other membrane proteins. *J. Biol. Chem.* **271,** 31196–31201 CrossRef Medline
73. Taura, T., Baba, T., Akiyama, Y., and Ito, K. (1993) Determinants of the quantity of the stable SecY complex in the *Escherichia coli* cell. *J. Bacteriol.* **175,** 7771–7775 CrossRef Medline
74. Thakur, K. G., Jaiswal, R. K., Shukla, J. K., Praveena, T., and Gopal, B. (2010) Over-expression and purification strategies for recombinant multi-protein oligomers: a case study of *Mycobacterium tuberculosis* σ/anti-σ factor protein complexes. *Protein Expr. Purif.* **74,** 223–230 CrossRef Medline
75. Gorynia, S., Matias, P. M., Bandeiras, T. M., Donner, P., and Carrondo, M. A. (2008) Cloning, expression, purification, crystallization and preliminary X-ray analysis of the human RuvBL1–RuvBL2 complex. *Acta Crystallogr. Sect. F Struct. Biol. Cryst. Commun.* **64,** 840–846 CrossRef Medline
76. Patoli, B. B., Winter, J. A., Patoli, A. A., Delahay, R. M., and Bunting, K. A. (2017) Co-expression and purification of the RadA recombinase with the RadB paralog from *Haloferax volcanii* yields heteromeric ring-like structures. *Microbiology* **163,** 1802–1811 CrossRef Medline
77. Kiefer, H., Krieger, J., Olszewski, J. D., Von Heijne, G., Prestwich, G. D., and Breer, H. (1996) Expression of an olfactory receptor in *Escherichia coli*: purification, reconstitution, and ligand binding. *Biochemistry* **35,** 16077–16084 CrossRef Medline
78. Kiefer, H., Vogel, R., and Maier, K. (2000) Bacterial expression of G-protein–coupled receptors: prediction of expression levels from sequence. *Receptors Channels* **7,** 109–119 Medline
79. Khow, O., and Suntrarachun, S. (2012) Strategies for production of active eukaryotic proteins in bacterial expression system. *Asian Pac. J. Trop. Biomed.* **2,** 159–162 CrossRef Medline
80. Monné, M., Chan, K. W., Slotboom, D.-J., and Kunji, E. R. (2005) Functional expression of eukaryotic membrane proteins in *Lactococcus lactis*. *Protein Sci.* **14,** 3048–3056 CrossRef Medline
81. Grisshammer, R., Duckworth, R., and Henderson, R. (1993) Expression of a rat neurotensin receptor in *Escherichia coli*. *Biochem. J.* **295,** 571–576 CrossRef Medline
82. Grisshammer, R., Little, J., and Aharony, D. (1994) Expression of rat NK-2 (neurokinin A) receptor in *E. coli*. *Receptors Channels* **2,** 295–302 Medline
83. Tucker, J., and Grisshammer, R. (1996) Purification of a rat neurotensin receptor expressed in *Escherichia coli*. *Biochem. J.* **317,** 891–899 CrossRef Medline
84. Welsch, S., Miller, S., Romero-Brey, I., Merz, A., Bleck, C. K., Walther, P., Fuller, S. D., Antony, C., Krijnse-Locker, J., and Bartenschlager, R. (2009) Composition and three-dimensional architecture of the dengue virus replication and assembly sites. *Cell Host Microbe* **5,** 365–375 CrossRef Medline
85. Chuang, C., Prasanth, K. R., and Nagy, P. D. (2017) The glycolytic pyruvate kinase is recruited directly into the viral replicase complex to generate ATP for RNA synthesis. *Cell Host Microbe* **22,** 639–652.e7 CrossRef Medline
86. Gebhard, L. G., Kaufman, S. B., and Gamarnik, A. V. (2012) Novel ATP-independent RNA annealing activity of the dengue virus NS3 helicase. *PLoS One* **7,** e36244 CrossRef Medline
87. Zhang, H., Rahman, S., Li, W., Fu, G., and Kaur, P. (2015) Characterization of a novel domain 'GATE' in the ABC protein DrrA and its role in drug efflux by the DrrAB complex. *Biochem. Biophys. Res. Commun.* **459,** 148–153 CrossRef Medline
88. Liu, R., and Sharom, F. J. (1996) Site-directed fluorescence labeling of P-glycoprotein on cysteine residues in the nucleotide binding domains. *Biochemistry* **35,** 11865–11873 CrossRef Medline